AD-A066 321 NORTHROP RESEARCH AND TECHNOLOGY CENTER PALOS VERDES --ETC F/G 20/5
INVESTIGATION OF GAIN AND ABSORPTION PROCESSES IN THE CADMIUM-M--ETC(U)
MAR 79 J B WEST, H KOMINE, E A STAPPAERTS N00014-77-C-0491

UNCLASSIFIED NRTC-79-6R NL

| OF |
AD
A066321

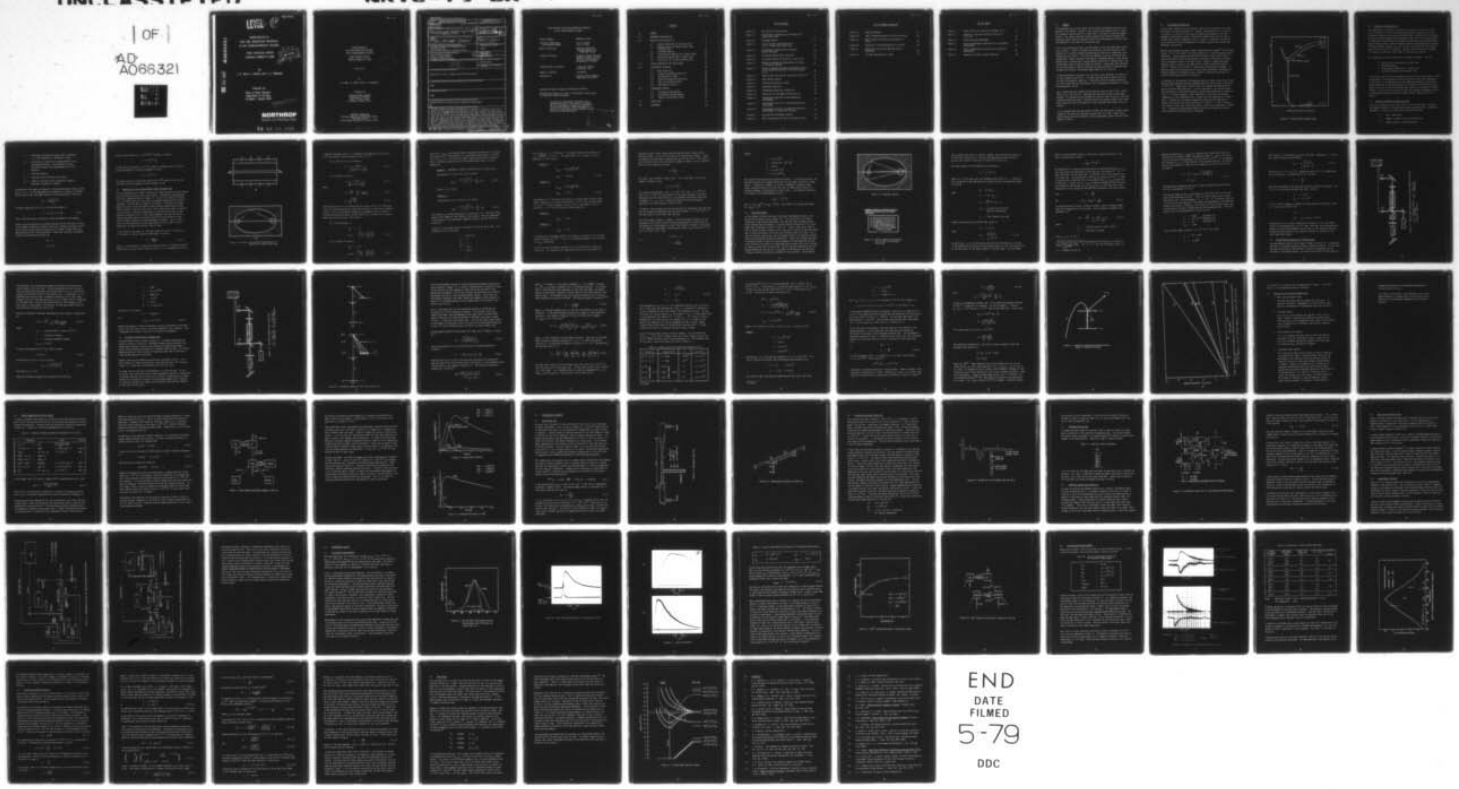

END
DATE
FILMED
5-79
DDC

NRTC 79-6R

LEVEL II (12)

AD A066321

DDC FILE COPY

INVESTIGATION OF GAIN AND ABSORPTION PROCESSES IN THE CADMIUM-MERCURY EXCIMER

FINAL TECHNICAL REPORT
CONTRACT N00014-77-C-0491

DDC
RECEIVED
MAR 26 1979
C

By

J. B. West, H. Komine, and E. A. Stappaerts

Prepared for

Office of Naval Research
Department of the Navy
Arlington, Virginia 22217

This document has been approved for public release and sale; its distribution is unlimited.

NORTHROP
Research and Technology Center

79 03 22 053

NRTC 79-6R

INVESTIGATION OF GAIN AND ABSORPTION PROCESSES IN THE CADMIUM-MERCURY EXCIMER

FINAL TECHNICAL REPORT

CONTRACT N00014-77-C-0491

DDC
RECEIVED
MAR 22 1979
C

March 1979

By

J. B. West, H. Komine, and E. A. Stappaerts

Prepared for

OFFICE OF NAVAL RESEARCH
DEPARTMENT OF THE NAVY
800 N. Quincy Street
Arlington, Virginia 22217

NORTHROP CORPORATION
Northrop Research and Technology Center
One Research Park
Palos Verdes Peninsula, California 90274

79 03 22 053

UNCLASSIFIED

SECURITY CLASSIFICATION OF THIS PAGE (When Data Entered)

REPORT DOCUMENTATION PAGE

READ INSTRUCTIONS BEFORE COMPLETING FORM

1. REPORT NUMBER: NRTC-79-6R	2. GOVT ACCESSION NO.
3. RECIPIENT'S CATALOG NUMBER	
4. TITLE (and Subtitle): INVESTIGATION OF GAIN AND ABSORPTION PROCESSES IN THE CADMIUM-MERCURY EXCIMER	5. TYPE OF REPORT & PERIOD COVERED: Final Technical Report 1 June 1977-28 Feb 1979
	6. PERFORMING ORG. REPORT NUMBER
7. AUTHOR(s): J. B. West, H. Komine, and E. A. Stappaerts	8. CONTRACT OR GRANT NUMBER(s): N00014-77-C-0491
9. PERFORMING ORGANIZATION NAME AND ADDRESS: Northrop Research and Technology Center, One Research Park, Palos Verdes Peninsula, California 90274	10. PROGRAM ELEMENT, PROJECT, TASK AREA & WORK UNIT NUMBERS: 121107
11. CONTROLLING OFFICE NAME AND ADDRESS: Office of Naval Research, Physics Program Office, Arlington, Virginia 22217	12. REPORT DATE: March 1979
	13. NUMBER OF PAGES: 69
14. MONITORING AGENCY NAME & ADDRESS (if different from Controlling Office): - (12) 78 p.	15. SECURITY CLASS. (of this report): Unclassified
	15a. DECLASSIFICATION/DOWNGRADING SCHEDULE: -

16. DISTRIBUTION STATEMENT (of this Report)

Approved for public release; distribution unlimited

17. DISTRIBUTION STATEMENT (of the abstract entered in Block 20, if different from Report)

None

18. SUPPLEMENTARY NOTES

None

19. KEY WORDS (Continue on reverse side if necessary and identify by block number)

Cadmium-Mercury, Excimer Lasers, Absorption Measurements

20. ABSTRACT (Continue on reverse side if necessary and identify by block number)

The CdHg excimer has received attention as a possible efficient visible laser medium. In the experiments described here, a pulsed, tunable laser was used to excite the Cd ~~($5\,^3P_1$)~~ atomic state which forms CdHg excimers in three body collisions with Hg and Ar. Gain and absorption measurements were performed by using an argon-ion laser to probe several wavelengths within the 470 nm excimer emission band. Net absorption was observed at all wavelengths investigated. Acoustic and thermal disturbances which might mimic absorption have been carefully considered and it is determined that these are not important. We conclude that the CdHg excimer exhibits net absorption within its 470 nm emission band. These results cast considerable doubt on the possibility of efficient laser action in CdHg.

DD FORM 1 JAN 73 1473 EDITION OF 1 NOV 65 IS OBSOLETE

407696

UNCLASSIFIED

SECURITY CLASSIFICATION OF THIS PAGE (When Data Entered)

INVESTIGATION OF GAIN AND ABSORPTION PROCESSES IN THE CADMIUM-MERCURY EXCIMER

Contract Number:	N00014-77-C-0491
Principal Investigator and Telephone Number:	Dr. J. B. West (213) 377-4811
Name of Contractor:	Northrop Corporation Northrop Research and Technology Center
Scientific Officer:	Director, Physics Programs Physical Sciences Division Office of Naval Research Department of the Navy
Effective Date of Contract:	1 June 1977 through 28 February 1979
Amount of Contract:	$72,828.00
Sponsored by:	Office of Naval Research Department of the Navy

Approved for public release; distribution unlimited.

Reproduction in whole or in part is permitted for any purpose of the United States Government.

The views and conclusions contained in this document are those of the authors and should not be interpreted as necessarily representing the official policies, either expressed or implied, of the Office of Naval Research or the United States Government.

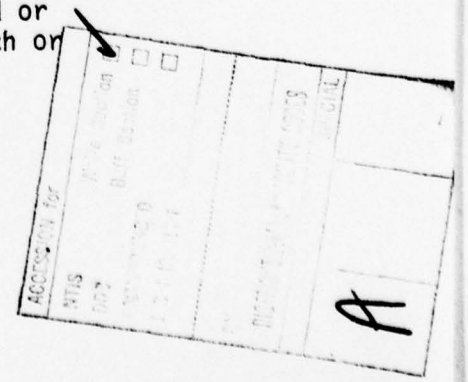

CONTENTS

1.0	SUMMARY		1
2.0	BACKGROUND AND OBJECTIVE		2
3.0	METHOD OF EXCITATION OF Cd		4
	3.1	General Expression for the Laser Gain	4
	3.2	Pumping with a Low Pressure Metal Vapor Discharge Lamp	6
	3.3	Flashlamp Pumping	12
	3.4	Single-Photon Pumping with a Tunable Laser	17
	3.5	Two-Photon Pumping with a Tunable Laser	20
	3.6	Conclusions of Excitation Method Study	31
4.0	KINETIC MODELING OF THE CdHg SYSTEM		33
5.0	EXPERIMENTAL APPARATUS		38
	5.1	Metal Vapor Cell	38
	5.2	Processing the Metal Vapor Cell	41
	5.3	Gain/Absorption Probe	43
	5.4	Detection System and Electronics	43
	5.5	326.1 nm Excitation Source	46
	5.6	Experimental Facility	46
6.0	EXPERIMENTAL RESULTS		50
	6.1	Fluorescence Measurements	50
	6.2	Gain/Absorption Measurements	57
	6.3	Acoustic and Thermal Effects	61
7.0	CONCLUSIONS		65
8.0	REFERENCES		68

LIST OF FIGURES

Figure 2.1	CdHg Potential Energy Curves	3
Figure 3.1	Two Possible Configurations for Pumping with a Metal Vapor Lamp	7
Figure 3.2	Flashlamp Pumping	13
Figure 3.3	Typical Spectral Distribution for a 1 μsec - 1 Joule Xenon Flash Lamp	13
Figure 3.4	Single-Photon Pumping with a Frequency Doubled Dye Laser	18
Figure 3.5	Two-Photon Pumping with a Dye Laser	21
Figure 3.6	Two-Photon Pumping of the 5p $^3P_1$ Level of Cd	22
Figure 3.7	Radiative Trapping and Photoionization Losses in Two-Photon Pumping	29
Figure 3.8	Effect of Radiative Trapping and Photoionization on the Population Build-Up in the 5p $^3P_1$ Level of Cd	30
Figure 4.1	CdHg Kinetics with Optical Excitation at 326.1 nm	35
Figure 4.2	CdHg Excimer Kinetics	37
Figure 4.3	Formation Efficiency of $CdHg^*$	37
Figure 5.1	CdHg Metal Vapor Cell	39
Figure 5.2	Thermocouple Locations on CdHg Cell	40
Figure 5.3	System for Filling Ampule with Hg and Cd	42
Figure 5.4	Differential Amplifier for Gain/Absorption Measurements	44
Figure 5.5	Experimental Facility for CdHg Gain/Absorption Experiments	47
Figure 5.6	Experimental Facility for CdHg Gain/Absorption Measurements at Higher Pump Energies	48
Figure 6.1	Cd_2 and CdHg Fluorescence Spectra	51
Figure 6.2	CdHg Fluorescence and 326.1 nm Excitation Pulse	52

LIST OF FIGURES (Continued)

Figure 6.3	CdHg Fluorescence	53
Figure 6.4	$CdHg^*$ Fluorescence Decay vs Excitation Energy	55
Figure 6.5	$CdHg^*$ Kinetics with Optical Excitation at 326 nm	56
Figure 6.6	Absorption in Excited Mixtures of Cd and Hg	58
Figure 6.7	Absorption in Laser Excited CdHg vapor vs Wavelength	60
Figure 7.1	Excited CdHg Electronic States	67

LIST OF TABLES

Table 3.1	Energy Levels and Transition Strengths for Cd	25
Table 4.1	Kinetics of CdHg with Optical Excitation of Cd ($5\ ^3P_1$)	33
Table 5.1	Argon-Ion Laser Wavelengths	43
Table 6.1	Typical Experimental Conditions for Fluorescence Measurements	54
Table 6.2	Typical Experimental Conditions for Absorption Measurements	57
Table 6.3	Absorption in Laser Excited CdHg Vapor	59

1.0 SUMMARY

The cadmium-mercury excimer ($CdHg^*$) has attracted considerable attention as a potential laser medium. Because of the transition wavelength (470 nm), there are a number of applications for a CdHg laser in the area of undersea communications. This report describes research conducted at Northrop Research and Technology Center (NRTC) to perform a definitive investigation of optical gain and absorption in the $CdHg^*$ 470 nm emission band.

Prior to any experimental work, various methods of exciting $CdHg^*$ were considered in detail. Electric discharge excitation was ruled out because of the possibility of creating unwanted excited species which would complicate interpretation of the results. Four different methods of optical excitation were contemplated: cadmium resonance lamp pumping, flashlamp pumping, single photon pumping with a tunable laser, and two-photon pumping with a tunable laser. The single photon laser excitation scheme was adopted. Using known rate constants for the CdHg system, a kinetics analysis was then performed to determine CdHg formation efficiencies and optimum number densities of Cd and Hg.

In these experiments, mixtures of Cd, Hg, and Ar were enclosed in a fused silica cell heated to about 900 K. A pulsed laser was used to excite the Cd on its 326.1 nm resonance transition. Three-body reactions between excited Cd, Hg, and Ar then form the CdHg excimer, and fluorescence is observed in a broad band centered at 470 nm.

Gain or absorption was probed with an argon-ion laser at 457.9, 472.7, 476.5, 496.5, 501.7, and 514.5 nm. Absorption was observed at each of these wavelengths. This absorption was strongest at the blue lines of the Ar^+ laser and decreased toward the green. Possible acoustic and thermal effects which could mimic absorption were considered and it was determined that these are not important.

It is concluded that the CdHg excimer exhibits net absorption at several wavelengths in the 470 nm fluorescence band and that it is not a viable laser medium unless absorption vanishes at other wavelengths within the band, which appears unlikely.

2.0 BACKGROUND AND OBJECTIVE

Excimer lasers based on rare gas halides, such as KrF, have demonstrated both high powers[1] and high efficiencies.[2] However, the wavelength of these lasers is typically in the ultraviolet spectral region where problems arise from atmospheric absorption by ozone. Additional problems arise from the lack of suitable laser optical components in the uv region. Furthermore, a laser directly emitting in the blue-green band is urgently required for several Navy underwater applications.

Mercury based diatomic excimers, such as cadmium-mercury (CdHg)[3-6] and thallium-mercury (TlHg)[7] have recently attracted attention as suitable blue-green laser candidates. These molecules show emission continua in the visible spectral region and should be efficiently excited in electrical discharges via excitation of metastable levels of the metal atom. Figure 2.1 shows approximate potential energy curves for the CdHg excimer, based on published spectral data.[3,6] However, little detail is known about these molecular systems. To evaluate these promising molecules as viable laser candidates, experiments to measure formation and quenching rates, and most importantly gain and/or absorption coefficients, must be carried out.

On the basis of the observed fluorescence spectra and decay times, Fournier and McGeoch[3] have estimated the CdHg stimulated emission cross section to be about 2×10^{-19} cm^2. McGeoch and Fournier[6] also have reported the observation of gain on the blue CdHg transition. In their experiments, the excited species were produced by a broad band flashlamp, and gain was probed with an argon-ion laser. A disturbing aspect of their experiment is that gain was measured independent of cell temperature over a range from room temperature to around 500 C. Pleasance and co-workers attempted to duplicate the experiment of McGeoch and Fournier, but they obtained a null result.[8] In order to resolve the question of gain due to the CdHg excimer, a definitive experiment is essential. Preferably the experimental method should be different than the one used by McGeoch and Fournier and by Pleasance.

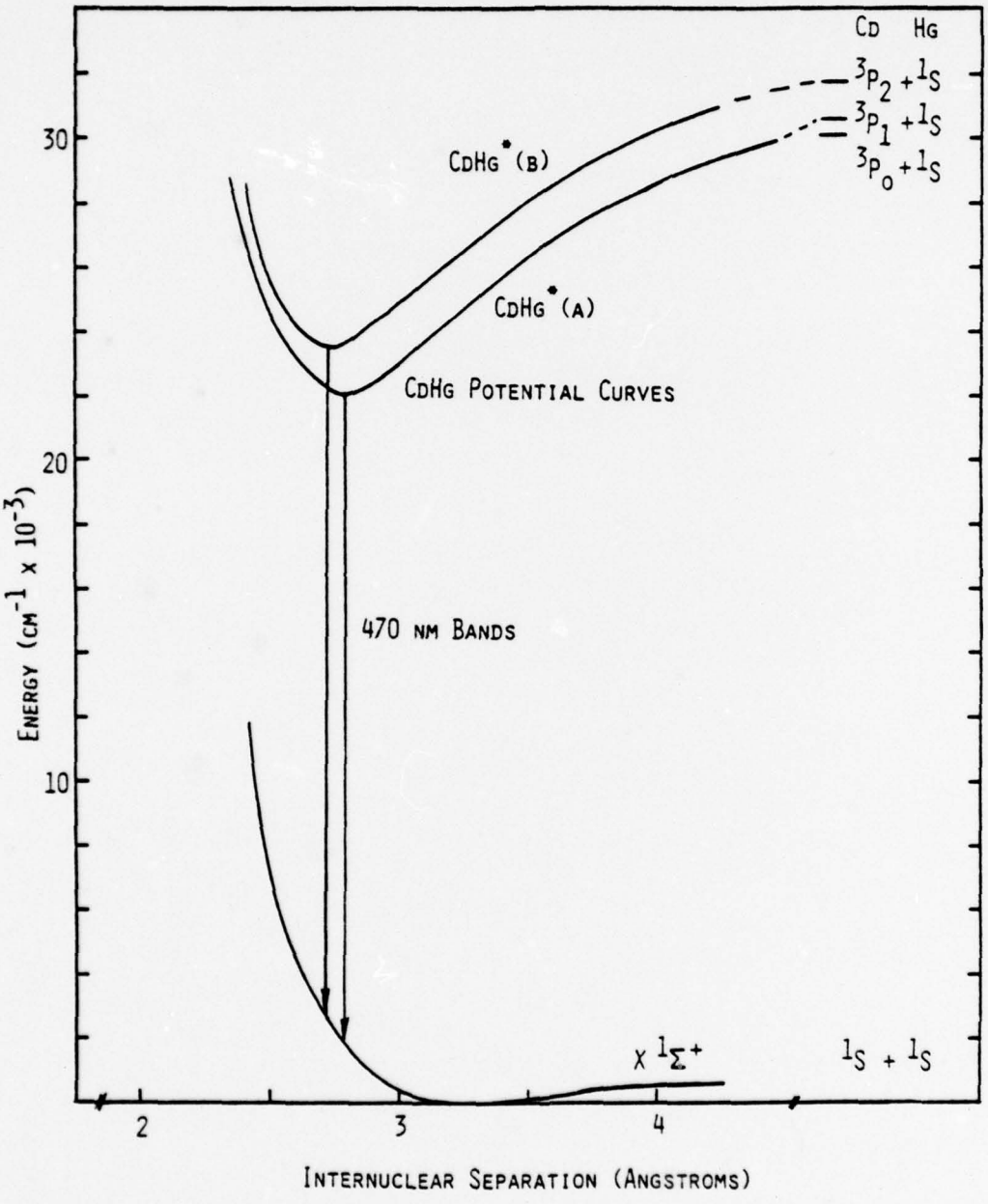

Figure 2.1 CdHg Potential Energy Curves

3.0 METHOD OF EXCITATION OF Cd

The CdHg excimer is formed by collisions of excited Cd with Hg in presence of a third body.[3,5] Prior to any experimental work, a detailed study was performed to determine the best excitation method. Both electrical discharge and optical pumping methods were considered. While Cd is excited efficiently in discharges, this technique was rejected for preliminary gain measurements because unknown effects such as electron quenching and nonselective excitation of other energetic species, e.g., Hg^* and Hg_2^*, could make the gain measurement results difficult to interpret. Optical excitation has the advantage of selectively exciting a given level of one particular species.

Four methods of optical excitation are considered in detail. They are:

1. Pumping with a low pressure Cd vapor lamp.
2. Flashlamp pumping.
3. Single-photon pumping with a tunable laser.
4. Two-photon pumping with a tunable laser.

In section 3.1 we will derive a general expression for the laser gain in terms of the energy in the optical excitation pulse and various other parameters. In Sections 3.2-3.5, expressions for the important parameters of each excitation scheme are derived and applied to the example of exciting the $5p\ ^3P_1$ level in Cd (this is the excited state that leads to the formation of $CdHg^*$). Finally, in Section 3.6, the merits of the four schemes are compared in terms of the gains obtainable with each of them, and their generality and complexity.

3.1 General Expression for the Laser Gain

We derive a simple but very useful relation for the laser gain in terms of the number of photons in the excitation pulse and various other fundamental parameters. We start by defining the following quantities:

g = Small signal gain.

q = Number of quanta in the excitation pulse.

N^* = Number density of excited molecules.

η_a = Efficiency with which the pump pulse is absorbed, i.e., the attenuation of the metallic vapor.

η_f = Efficiency of formation of excited molecules from the absorbed photons. This parameter is found from the solution of the approximate set of rate equations.

σ = Gain cross section.

A = Area over which excitation takes place.

L_a = Length of the vapor zone or absorption length of the vapor, whichever is shorter.

By definition, the number of molecules in the desired excited state is equal to $\eta_a \times \eta_f \times q$. If the pump photons are absorbed in a length L_a uniformly over an area A, then the number density of excited molecules is given by:

$$N^* = \frac{\eta_a \times \eta_f \times q}{A\, L_a}$$

The small signal gain $g = \sigma N^* L_a$ can thus be written as

$$g = \eta_a \times \eta_f \times \sigma \times \frac{q}{A} \qquad (3.1.1)$$

This is the final result; note that it does not depend on the length L_a.

We will use this expression to estimate the gain of the CdHg laser in terms of the number of photons available at 326.1 nm. Assume an excitation pulse which is much shorter than the excited state lifetime of CdHg, which has been measured to be a few microseconds.[3] Under this condition, reasonable values for the efficiency factors are

$$\eta_a \simeq 1$$

$$\eta_f \simeq 0.5$$

Using a cross section of 2×10^{-19} cm^2,[5] the gain is given by

$$g = 1 \times 10^{-19} \frac{q}{A}$$

If the area of excitation is 10^{-2} cm^2, which is probably about as small as one can go because of practical problems, we find

$$g = 1 \times 10^{-17} q \ .$$

This means that for a single pass gain of 10%, 10^{16} quanta at 326.1 nm are required, which corresponds to a pulse energy of 6 mJ.

3.2 Pumping with a Low Pressure Metal Vapor Discharge Lamp

The first method we will study is the use of a lamp containing the same species as the one to be excited in the lasing medium. Two possible configurations for such a scheme are shown in Figure 3.1. In the first geometry[9] (Figure 3.1a), the lamp consists of two coaxial cylinders between which the vapor is contained. The gain tube is placed in the center. To obtain large output powers from such a lamp, the radii of the cylinders should be much larger than the radius of the gain tube, which itself should be as small as possible since the gain is inversely proportional to the area of this tube, as was derived in Equation (3.1.1). In the second geometry, the lamp and the gain tube are cylinders which are placed in the foci of an elliptical cavity which is highly reflective at the wavelength of interest. We will give a very simplified derivation of the output power of such a lamp, for both geometries, and apply the results to the Cd lamp.

If the volume of the lamp is V, the vapor density N, and if a fraction of f of the vapor is excited, then the output power is given by

$$P = \frac{NVfh\nu}{\tau/g} \qquad (3.2.1)$$

where τ is the radiative lifetime of the species and g is a trapping factor[10] which has a value less than or equal to unity. If it is assumed that the line

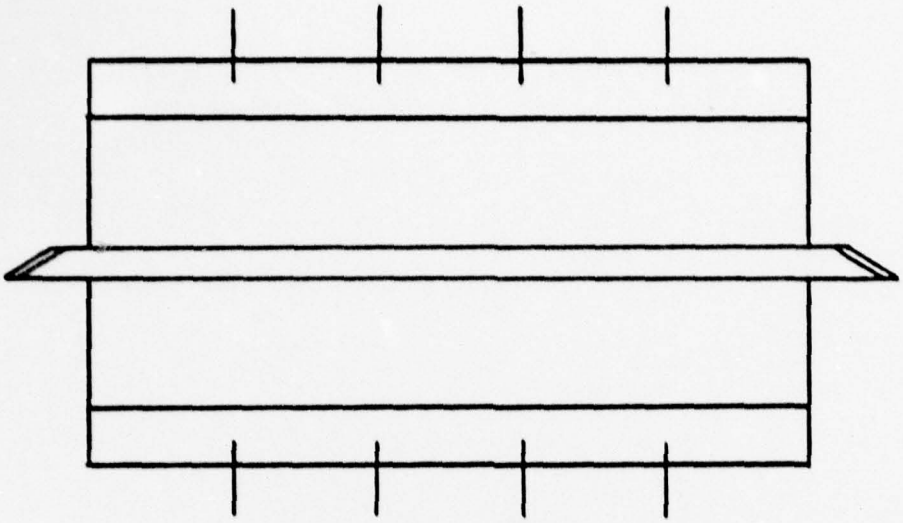

(a)

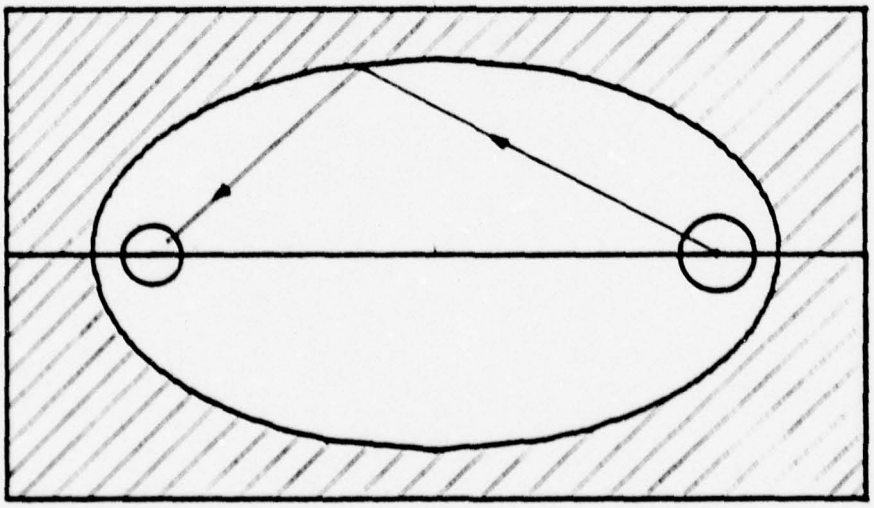

(b)

Figure 3.1 (a),(b) Two Possible Configurations for Pumping with a Metal Vapor Lamp

is Doppler broadened, which is a reasonable approximation at the low densities considered,[11] then the expression for g is:[10]

For an infinite slab of thickness t:

$$g = \frac{1.875}{k_o t \left[\pi \log \left(\frac{1}{2} k_o t\right)\right]^{\frac{1}{2}}} \tag{3.2.2}$$

For a cylinder of radius R:

$$g = \frac{1.6}{\left[k_o R \pi \log (k_o R)\right]^{\frac{1}{2}}} \tag{3.2.3}$$

where

$$k_o = \frac{\lambda^3 N}{8\pi} \quad \frac{g_2}{g_1} \quad \frac{1}{\sqrt{\pi}\, v_o t} \tag{3.2.4}$$

$$v_o = \sqrt{\frac{2kT}{M}} \tag{3.2.5}$$

The expression for g is valid only when its value is equal to or less than unity; for densities below the value such that this is the case, no trapping occurs. This critical density depends on the geometry, and is found by solving the expressions above for the value of $k_o t$, respectively, $k_o R$ which makes the value of g unity. The result is

For a slab thickness t:

$$k_o t \simeq 2.8$$

$$N_{crit} = \frac{125\, v_o}{\lambda^3 t} \left(\frac{g_1}{g_2}\right)_T \tag{3.2.6}$$

For a cylinder of radius R:

$$k_o R \simeq 1.8$$

$$N_{crit} = \frac{80\, v_o}{\lambda^3 R} \left(\frac{g_1}{g_2}\right)_T \tag{3.2.7}$$

Since for $N > N_{crit}$ the trapping factor g becomes less than unity, and since the output power is proportional to g, the maximum output power is obtained for $N = N_{crit}$, i.e., at the density where trapping starts being important. We will now derive expressions for this maximum output power, for both geometries.

Geometry I (Resembles a slab of thickness R_2-R_1 if $R_2-R_1 \ll R_{av}$)

Substitution of (3.2.6) into (3.2.1) yields:

$$P_{max} = \frac{1.5 \times 10^{-20} \, v_o}{\lambda^4} \frac{g_1}{g_2} RLf \qquad (3.2.8)$$

where $R = (R_1 + R_2)/2$

Geometry II

Substitution of (3.2.7) into (3.2.1) yields:

$$P_{max} = \frac{5.0 \times 10^{-21} \, v_o}{\lambda^4} \frac{g_1}{g_2} RLf \qquad (3.2.9)$$

The velocity v_o in these expressions is given by (3.2.5). Note that these powers do not depend on the lifetime of the species. The only dependence on the species is via wavelength, degeneracy factors and the fraction of excitation.

We now will apply these results to the 326.1 nm line of the Cd lamp. The parameters for this case are:

λ = 326.1 nm

g_1 = 1

g_2 = 3

M = 112.4

T = 600 K

This yields $v_0 = 3.2 \times 10^4$ cm/sec. The Doppler width at this temperature $\Delta\nu_D = \sqrt{kT/m\lambda^2} = 0.02\ cm^{-1}$. The output power of a Cd lamp in the two geometries is then given by:

Geometry I

$$N_{crit} = \frac{0.8 \times 10^{14}\ cm^{-3}}{t}$$

$$P_{max} = 140\ fRL \qquad (3.2.10)$$

Geometry II

$$N_{crit} = \frac{0.5 \times 10^{14}\ cm^{-3}}{R}$$

$$P_{max} = 47\ fRL \qquad (3.2.11)$$

Experimentally[11] it has been found that the uv output power of these lamps shows a maximum for a certain tube diameter. For Cd, this optimum diameter is 2.5 cm.[11] For this diameter, and for a 50-cm long length, using an f value[11] of 3×10^{-3}, we find that the output powers are:

Geometry I

$$P_{max} \simeq 50\ W$$

Geometry II

$$P_{max} \simeq 20\ W$$

In Reference 11, the number density for maximum uv production in Cd has been found to be about $10^{14}\ cm^{-3}$. This is in reasonable agreement with the value for N_{crit} found above.

For this case of CW pumping, Equation (3.1.1) for the gain is actually of little use. This expression is indeed mainly useful for cases where the

excitation pulse is much shorter than the excited state lifetime of the molecules formed. It can still be used in an indirect way, however. Since the molecular excited state population can only build up for a time equal to the lifetime of this state, an effective number of photons in the excitation "pulse" can be defined as follows:

$$q = \frac{P\tau}{h\nu_o}$$

For $CdHg^*$, the lifetime[3] is about 3 μsec. For a lamp power of 50 W, the number of photons is then

$$q = 2.5 \times 20^{14}$$

For a typical gas mixture: $[Cd] = 5 \times 10^{17}$ cm^{-3}, $[Hg] = 2 \times 10^{18}$ cm^{-3}, and $[M] = 2 \times 10^{19}$ cm^{-3}, the solution of the rate equations in Section 4 shows that with this definition of q, the formation efficiency can be 50% or greater, i.e., $\eta_f \geq 0.5$. Assuming a spatially uniform excitation, Equation (3.1.1) then predicts a gain of 0.25%.

In reality, the excitation will not be uniform, but the photons from the lamp will be resonantly absorbed by the high density vapor ($\simeq 5 \times 10^{17}$ cm^{-3}) in the laser tube in a thin shell near the wall.

For a gain tube of radius r, length L, filled with vapor at density N, the thickness of this shell can be calculated approximately by saying that all the photons will be absorbed in a shell that contains a number of atoms equal to the number of pump photons (the absorption depth $1/k_o$ is equal to 10^{-4} cm at $N = 5 \times 10^{17}$ cm^{-3}). Thus

$$2\pi r \Delta N L = q$$

or

$$\Delta = \frac{q}{2\pi r N L}$$

Example:

$$q = 2.5 \times 10^{14}$$

$$r = 0.06 \text{ xm } (A = 0.01 \text{ cm}^2)$$

$$L = 50 \text{ cm}$$

$$N = 5 \times 10^{17} \text{ cm}^{-3}$$

$$\Delta = 0.3 \times 10^{-4} \text{ cm}$$

This spatial nonuniformity has several bad effects. In the excited shell, the molecular excited state number density will be very high, resulting in large "gains". Diffraction, however, will make it impossible to measure these gains, and amplification will only occur over a length roughly equal to a confocal parameter corresponding to a waist size Δ. The effective amplification length is thus approximately given by

$$L_{eff} \simeq 2\pi\Delta^2/\lambda$$

For $\Delta = 0.03 \times 10^{-4}$ cm, $L_{eff} = 10^{-4}$cm. This result in a maximum gain equal to $\sigma NL_{eff} = 10^{-5}$.

3.3 Flashlamp Pumping

In this scheme, the gain tube and a high power flashlamp are placed in the foci of an elliptical cavity (Figure 3.2). This cavity has to be highly reflecting at the desired wavelength, such that the light can make several passes through the laser medium. A typical spectral distribution for a high power xenon flashlamp is shown in Figure 3.3. Clearly, when such a lamp is used to excite an atomic species, only a very small fraction of the lamp energy goes in atomic excitation, while the rest eventually ends up as heat. As in the case of metal vapor lamps, only the energy emitted in a molecular excited state lifetime determines the gain obtainable. Longer pulse lengths may make it possible though to reach the lasing threshold in cases where the excited state lifetime is too short to allow enough cavity round trips in one lifetime to reach an overall gain of about e^{30}. We will derive an expression for the energy absorbed by the atoms in a time equal to the molecular excited state lifetime, assuming a Lorentzian lineshape for the absorbers. The procedure

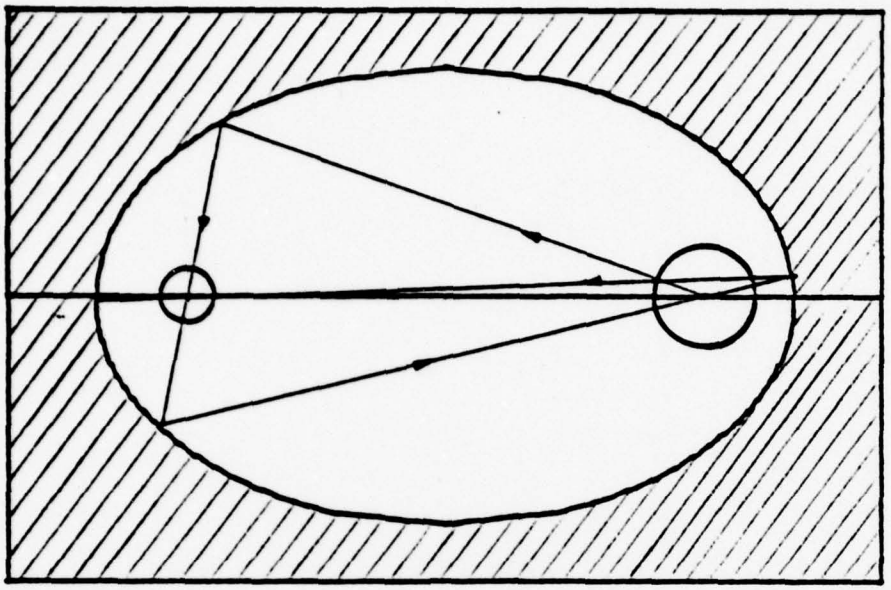

Figure 3.2 Flashlamp Pumping

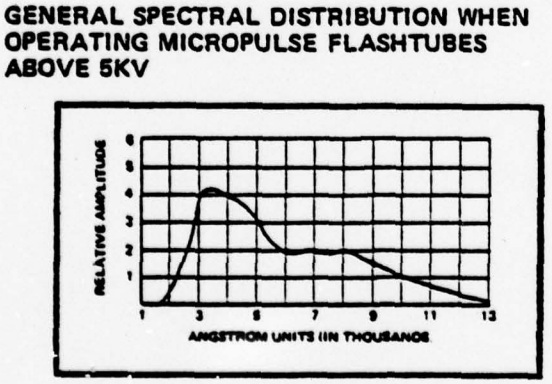

Figure 3.3 Typical Spectral Distribution for a 1 μsec -1 Joule Xenon Flash Lamp

used to obtain this result is general, however, and can easily be adapted to an arbitrary lineshape (e.g., one that has been measured experimentally). We apply the results to excitation of the 5p $^3P_1$ level of Cd.

The output energy of the flashlamp can be written as

$$E_L = \int_0^\infty E(\nu)\, d\nu$$

where $E(\nu)$ is the output per unit bandwidth (see Figure 3.3). If radiation over a bandwidth B gets absorbed by the atomic species, the deposited energy is given by

$$E_D = E(\nu)\, B\, \eta_t$$

where

$$\eta_t = 1 \text{ for } \tau_{ES} > \tau_L$$

$$\eta_t = \frac{\tau_{ES}}{\tau_L} \text{ for } \tau_{ES} < \tau_L$$

τ_{ES} = Lifetime of the excited state of the molecule

τ_L = Pulse length of the lamp

Another more useful way of writing this energy is:

$$E_D = E_L\, \eta_D\, \eta_t$$

where

$$\eta_D = \frac{E(\nu_o)\, B}{\int_0^\infty E(\nu)\, d\nu} \qquad (3.3.1)$$

By definition, η_D is the efficiency with which the lamp energy is utilized. If the absorption cross section of the atomic species is $\sigma(\nu)$, the reflectivity of the cavity wall R, the inner diameter of the gain tube d, and the number

density of the absorbing species N, then after n passes the energy of the lamp is attenuated by a factor

$$\alpha = \left(R e^{-\sigma(\nu) N d} \right)^n$$

The bandwidth B is found by requiring that at the maximum detuning $|\nu_o - \nu|_{max}$ from line center the attenuation of the vapor be, for example, e^{-1}. At each reflection from the cavity wall, a fraction (1-R) of the incident radiation gets lost. One possible way of defining a maximum value for n is then to require that no more than 50% of the radiation at $|\nu_o - \nu|_{max}$ be absorbed by the walls. A value for $|\nu_o - \nu|_{max}$ can then be obtained by requiring that the attenuation coefficient $\sigma \left(|\nu_o - \nu|_{max} \right) Nd \simeq 1$, such that most of the energy which is not absorbed by the wall gets deposited in the laser medium*.

Thus

$$n \simeq \frac{0.5}{1-R}$$

and

$$\alpha \left(|\nu_o - \nu|_{max} \right) \simeq \frac{1}{Nnd} \qquad (3.3.2)$$

To proceed beyond this point, we have to assume a certain frequency dependence for the absorption cross section. For a Lorentzian lineshape, this dependence is[12]

$$\sigma(\nu) = \frac{r_e f}{2} \frac{\Delta\nu}{(\nu_o - \nu)^2 + \left(\frac{\Delta\nu}{2}\right)^2} \qquad (3.3.3)$$

where

r_e = electron radius = 2.818×10^{13} cm

f = oscillator strength

with ν_o, ν, $\Delta\nu$ in [cm^{-1}].

---

*The exact expression for the energy deposition efficiency in n passes is $\frac{R(1-e^{-\sigma ND})(1-R^n e^{-\sigma Nnd})}{1-Re^{-\sigma Nd}}$. For $0.7 < R < 0.99$, the efficiency varies, as $n \to \infty$, between 50% and 70%.

Because the detuning $|\nu_o - \nu|_{max}$ will always be much larger than the atomic linewidth and the Doppler width, the apparent spread in ν_o due to the velocity of the atoms can be neglected, and also the term $(\Delta\nu/2)^2$ can be neglected with respect to $(\nu_o - \nu)^2$ when solving for the maximum detuning. The expression for this detuning is then found by combining (3.3.2) and (3.3.3) with the result

$$B = 2|\nu_o - \nu|_{max} = \left[\frac{r_e f\, Nd\, \Delta\nu}{(1-R)}\right]^{\frac{1}{2}} \propto d^{\frac{1}{2}} (\Delta\nu)^{\frac{1}{2}} \qquad (3.3.4)$$

The energy which determines the gain if found by substituting this expression for the bandwidth in (3.3.1).

We now apply these results to the pumping of the $5p\ ^3P_1$ level of Cd, which leads to the formation of $CdHg^*$. Due to a lack of data, we will assume that the Cd line is self-broadened, i.e., $\Delta\nu = kN$. If it turns out that this is not the case, then because of the square root dependence of the deposited energy on the atomic linewidth $\Delta\nu$, this energy will go up by the square root of the ratio of the real linewidth and the self-broadened width. The parameters for the self-broadened 326.1 nm Cd line are:

f	=	0.0019	(Reference 13)
k	=	5.6×10^{-20}	(Reference 13)
R	=	0.9	(Reference 14)
τ_{ES}	=	3 μsec	

For an atomic number density $N = 5 \times 10^{17}\ cm^{-3}$, this yields

$$\Delta\nu = kN = 0.028$$

$$B = 8.6\sqrt{d}$$

From Figure 3.3, the quantity η_D can be calculated. Because $E(\lambda)$ is given, this quantity should be rewritten as

$$\eta_D = \frac{E(\lambda_o)\, B}{\int_0^\infty \frac{1}{\lambda^2} E(\lambda)\, d\lambda} \qquad (3.3.5)$$

The result is $\eta_D \simeq 4.5 \times 10^{-5}\ B$. Because the gain (3.1.1) is proportional to q/A, and E_D or q is proportional to $d^{\frac{1}{2}}$, we find

$$g \propto \frac{1}{d^{\frac{1}{2}}}$$

and thus the diameter of the gain tube should be as small as possible. For d = 0.1 cm, which should be about the limit, we find

$$B = 2.7\ cm^{-1}$$

$$\eta_D = 1.2 \times 10^{-4}$$

If, as a typical example, a Novatron 734 lamp would be used with E_L = 10J, τ_L = 1.5 μsec, we finally find

$$\eta_t = 1$$

$$E_D = E_L \times \eta_D \times \eta_t = 1.2\ mJ$$

According to (3.1.1), using a formation efficiency η_f = 0.5, this would result in an estimated gain of 2% for CdHg. Note that since the absorption length is several tube diameters long for most of the radiation that gets absorbed, the excitation will be spatially uniform, in contrast to the metal-vapor-lamp scheme.

3.4 Single-Photon Pumping with a Tunable Laser

The experimental setup for this scheme is shown in Figure 3.4. A high power dye laser is frequency doubled to produce radiation at 326 nm. For dye laser energies on the order of 100 mJ/pulse, as much as 10 mJ/pulse will be available in the doubled output. By tuning the dye laser off the center of

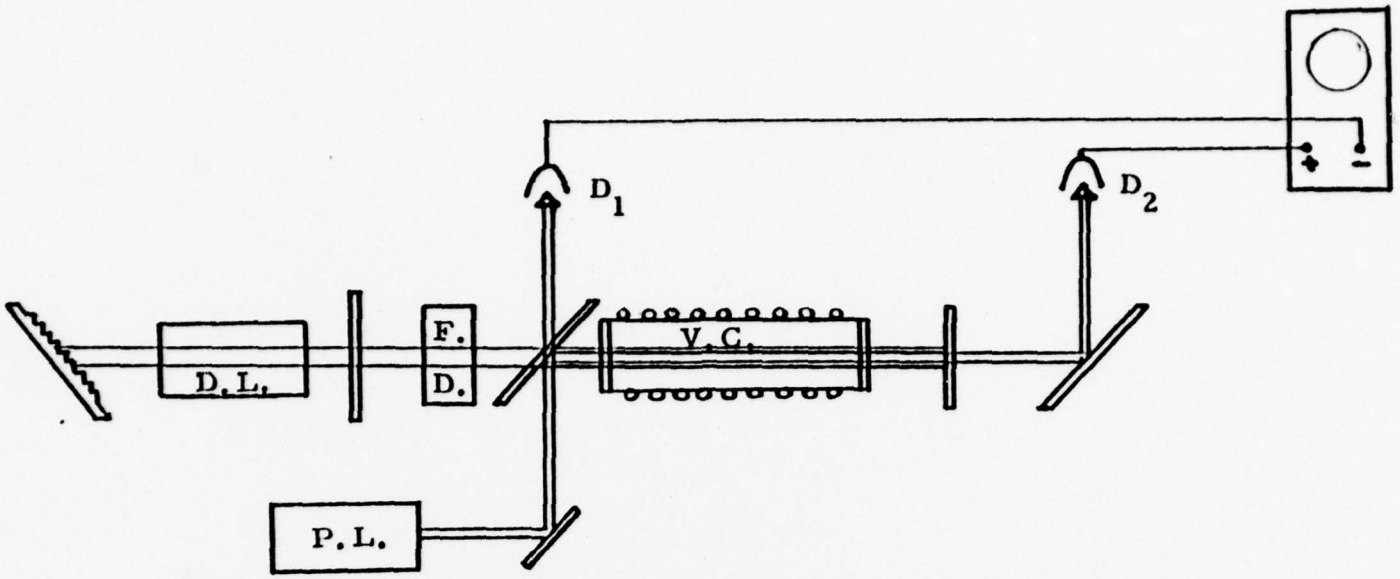

Figure 3.4 Single-Photon Pumping with a Frequency Doubled Dye Laser

F.D. = Frequency Doubler V.C. = Vapor Cell
D.L. = Dye Laser P.L. = Probe Laser
D_1 and D_2 = Detectors

the absorption line, the absorption depth of the vapor can be made equal to the length of the vapor zone. The gain obtainable with this scheme is found by substituting the energy of the pump laser in (3.1.1), taking into account the efficiency factor η_t (see Section 3.3). As an example, for an absorption efficiency of 63%, a formation efficiency of 50%, and a pump energy of 10 mJ in a 100 nsec long pulse (η_t=1), a gain of 10% is predicted for the CdHg laser. We will derive expressions for the frequency of the pump laser or, equivalently, its detuning. We then apply these results to the excitation of the 5p $^3P_1$ level in Cd.

Assuming a Lorentzian lineshape, the absorption cross section is then given by:

$$\sigma(\nu) = \frac{r_e f}{2} \frac{\Delta\nu}{(\nu_o - \nu)^2 + \left(\frac{\Delta\nu}{2}\right)^2} \qquad (3.4.1)$$

where:

r_e = electron radius = 2.818×10^{-13} cm

f = oscillator strength

$\Delta\nu$ = pressure broadened linewidth

$\nu_o, \nu, \Delta\nu$ in cm^{-1}

To obtain an absorption of e^{-1} (η_a = 63%), we need:

$$\sigma(\nu)\, NL = 1 \qquad (3.4.2)$$

Substitution of (3.4.1) in (3.4.2) yields:

$$|\nu_o - \nu| = \left[\frac{r_e f\, NL\, \Delta\nu}{2}\right]^{\frac{1}{2}} \qquad (3.4.3)$$

Note that $|\nu_o - \nu| \propto \Delta\nu^{\frac{1}{2}}$.

Using the following parameters for excitation of Cd (5p $^3P_1$),

$$f = .0019$$

$$\Delta\nu = 5.6 \times 10^{-20} N$$

$$\nu_o = 30665 \text{ cm}^{-1}$$

$$A = .01 \text{ cm}^2$$

$$L = 50 \text{ cm}$$

$$N = 5 \times 10^{17} \text{ cm}^{-3}$$

Yields for a 10 mJ pulse,

$$\Delta\nu = 0.028 \text{ cm}^{-1}$$

and

$$|\nu_o - \nu| = 13.7 \text{ cm}^{-1} \qquad (3.4.4)$$

Because the pumping is done off-resonance, the only requirement on the bandwidth of the dye laser is that it be narrow compared to this detuning. Thus, a bandwidth on the order of one cm^{-1} will usually be acceptable.

3.5 Two-Photon Pumping with a Tunable Laser

The experimental setup is shown in Figure 3.5. A diagram describing the process is shown in Figure 3.6. Multiphoton pumping may be desirable over single photon pumping in certain cases because the pumping wavelength is longer, thus eliminating the need for a frequency doubling step. As a result, pumping energies at least an order of magnitude higher than in the case of single photon pumping are available.

However, there may be problems associated with two-photon pumping. After being pumped to a higher excited state, some atoms may decay into undesired states, i.e., there may be a branching ratio less than unity.

For atoms like Cd, the sum of three photons is in the continuum. At the relatively high intensities used in these experiments (the gain is proportional to pumping intensity, see (3.1.1)), this can result in photoionization losses caused by the ionization of atoms in the two-photon pumped state. Because of radiative trapping, this effect can be important even when the lifetime of that state is very short.

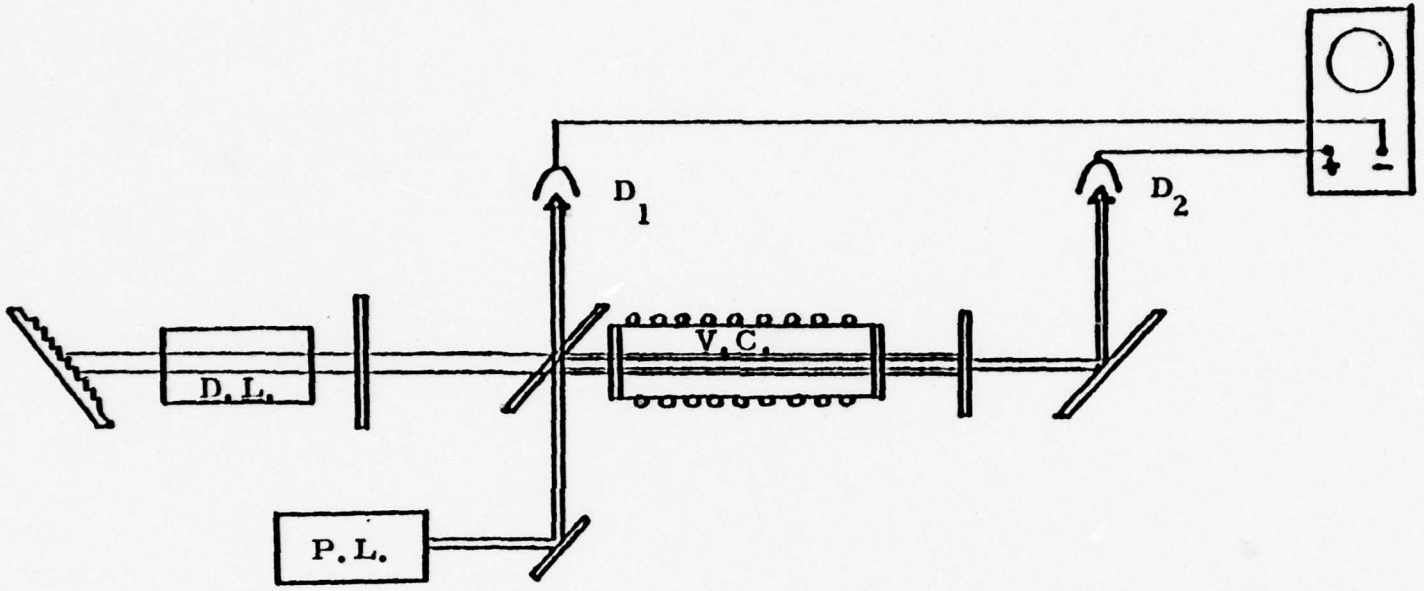

Figure 3.5 Two-Photon Pumping with a Dye Laser

V.C. = Vapor Cell D.L. = Dye Laser
P.L. = Probe Laser D_1 and D_2 = Detectors

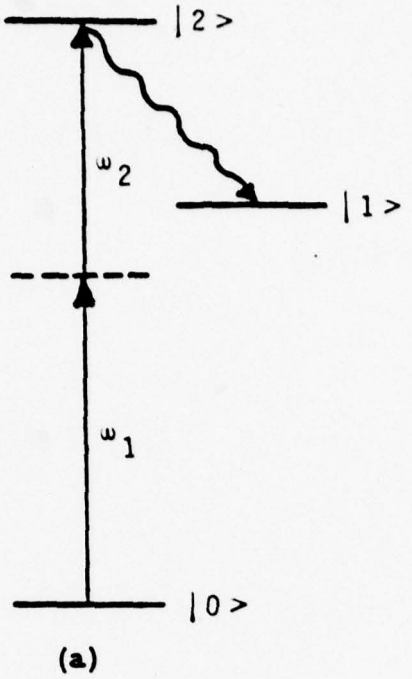

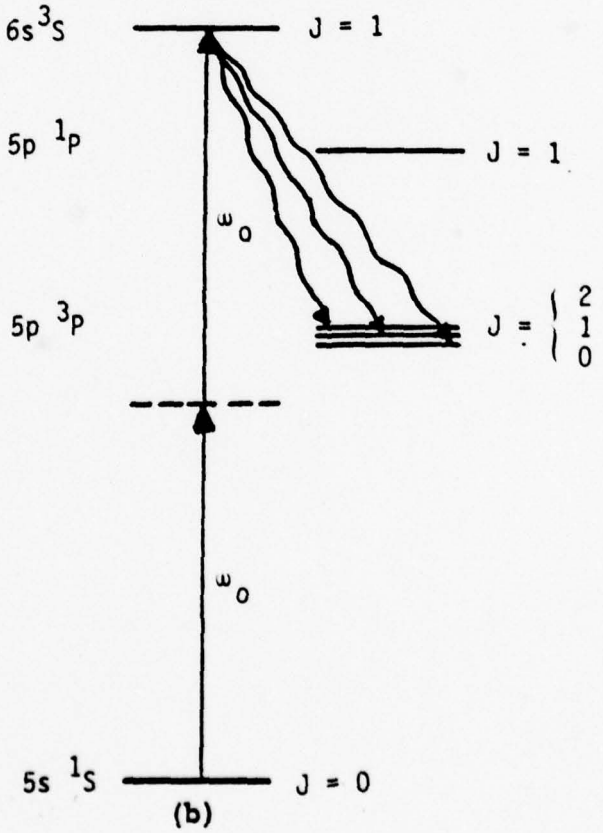

Figure 3.6 Two-Photon Pumping of the 5p $^3P_1$ Level of Cd

Since the experimental setups for single-photon and two-photon pumping are nearly identical, however, it is usually a simple matter to compare the pumping efficiencies of both schemes by simply tuning the dye laser to the appropriate wavelengths. We will not consider the case where two different wavelengths are used in the two-photon pumping process. Aside from the experimental complexity, the lower intensities needed with this method are usually of no advantage because of the proportionality of the gain to intensity [see (3.1.1)].

We will give expressions for the two-photon absorption coefficient and the Stark shift of the two-photon resonance. These dynamic shifts are usually very small, but not necessarily for atoms like Cd for which high pumping intensities are required because of the small oscillator strength of the $0 \rightarrow 1$ transition (see Figure 3.6a). We will then apply these results to the example of populating the $5p\ ^3P_1$ level in Cd by two-photon absorption to the $6s\ ^3S$ level followed by decay to the $5p\ ^3P_1$ state (Figure 3.6b).

The two-photon absorption coefficient for a vapor zone of length L is given by:[15]

$$\eta_a = \frac{W^{(2)}\, NL\, h\nu_o / I}{1 + W^{(2)}\, NL\, h\nu_o / I} \qquad (3.5.1)$$

The gain expression (3.1.1) can for the case of two-photon pumping be written as

$$g = 0.5\, \eta_a\, \eta_f\, \eta_t\, \eta_B\, \sigma\, \frac{q}{A} \qquad (3.5.2)$$

where the factor 0.5 is due to the fact that two photons are required to make one atom in the final excited state, the factor η_B is the branching ratio, and the factor η_t was defined in Section 3.3. The two-photon absorption probability is given by:[16]

$$W^{(2)} = \frac{\sqrt{2\pi}\, \eta_o^{\,2}\, \mu_{01}^{\,2}\, \mu_{12}^{\,2}\, I^2}{\hbar^4\, (\omega_{10} - \omega_o)^2\, \delta} \qquad (3.5.3)$$

where η_o = 377 ohms, δ is the laser linewidth ($\delta \equiv 1.2 \times$ FWHM) in radians, μ_{01} and μ_{12} are matrix elements, and I is the pump intensity. This expression is valid when the laser bandwidth is wider than the atomic and Doppler widths, and the atomic linewidth is larger than the axial mode spacing of the tunable laser. At reasonably high total pressures (several tens of Torrs), these conditions are usually satisfied. The focusing length is given by:[12,16]

$$Z_f = \frac{d}{4\sqrt{\delta n}} \tag{3.5.4}$$

where d is the beam diameter and δn is the Kerr contribution to the index of refraction. If the pump radiation consists of a number of axial modes with spacing $\Delta\omega$, the index of refraction for the m'th mode (with frequency $\omega = \omega_{20}/2 + \Delta\omega$) is given by:[15]

$$(n-1) = \frac{\eta_o N \mu_{01}^2 \mu_{12}^2 I}{2\epsilon_o \hbar^3 (\omega_{10} - \omega_o)^2} \times \frac{m\Delta\omega}{(m\Delta\omega)^2 + \frac{\gamma}{2}^2} \tag{3.5.5}$$

where γ is the linewidth of the forbidden transition. Note that for the mode which is exactly two-photon resonant (m = 0), (n -1), while the maximum value of (n - 1) occurs for the modes for which $(m\Delta\omega) \simeq \gamma/2$. The expression for the Stark shift is:[17]

$$\Delta\Omega_s = \frac{\eta_o I}{\hbar^2} \times \left[\sum_k \frac{\mu_{2K}^2 \omega_{k2}}{\omega_{k2}^2 - \omega_o^2} - \sum_k \frac{\mu_{0k}^2 \omega_{k0}}{\omega_{k0}^2 - \omega_o^2} \right] \tag{3.5.6}$$

The sums over k refer to all the allowed transitions starting in level 2 for the first sum and 0 for the second sum. In many cases the oscillator strength f_{12} is not known. It is therefore useful to study the dependence of η_a, Z_f and $\Delta\Omega_s$ on this quantity. From (3.5.1), (3.5.5), and (3.5.6):

$$\eta_a \propto \frac{f_{12} I}{1 + c f_{12} I}$$

$$n - 1 \propto f_{12} I \qquad (3.5.7)$$

$$\Delta\Omega_s \propto f_{12} I$$

The dependence of $\Delta\Omega_s$ on $f_{12} I$ is not immediately obvious, but it turns out that in many cases the contribution of the $2 \rightarrow 1$ transition is dominant or at least comparable to the other terms in the summations (3.5.6). We thus find that, for a given value of η_a, the product of $f_{12} I$ is fixed, which then in turn determines the values of $(n - 1)$ and $\Delta\Omega_s$. As a result, an exact knowledge of f_{12} is not crucial; for example, if f_{12} is a factor of two smaller than expected, this can be compensated for by focusing tighter, without affecting the index of refraction and the Stark shift. A higher intensity may result in increased ionization losses, however.

We will now apply these results to the Cd example. For the transitions $5p\ ^3P_{0,1,2} \rightarrow 6s\ ^3S$ we will assume a total oscillator strength of one, and split it among the three lines following Reference 18. The parameters that will be used in the calculations are listed in Table 3.1.

Table 3.1 Energy Levels and Transition Strengths for Cd

Transition	Energy (cm^{-1})	f	$\lvert\mu\rvert$ (C-m)
$5s\ ^1S - 5p\ ^3P_1$	0 - 30656	.0019[8]	7.0×10^{-31}
$5s\ ^1S - 5p\ ^1P$	0 - 43692	.92[13]	1.3×10^{-29}
$5p\ ^3P_0$	30114	.13*	7.0×10^{-30}*
$5p\ ^3P_1$ - $6s\ ^3S$	30656 - 51484	.25*	1.0×10^{-29}*
$5p\ ^3P_2$	31827	.62*	1.6×10^{-29}*

*Estimates

To calculate $W^{(2)}$ and $(n - 1)$, we use the path: $5s\ ^1S \rightarrow 5p\ ^3P_1 \rightarrow 6s\ ^3S$ $5p\ ^3P_1 \rightarrow 5s\ ^1S$. To calculate $\Delta\Omega_s$, we use the transitions $6s\ ^1S \rightarrow 5p\ ^3P_{0,1,2}$ in the first sum, and the transition $5s\ ^1S \rightarrow 5p\ ^1P$ in the second sum in (2.4.6). The results of these calculations are:

$$W^{(2)} = 10^{-10}\ I^2/\delta$$

$$\eta_a = \frac{5 \times 10^{-29}\ NL\ I/\delta}{1 + 5 \times 10^{-29}\ NL\ I/\delta}$$

$$n - 1 = 6 \times 10^{-35}\ N\ I \times \frac{m\Delta\omega}{(m\Delta\omega)^2 + \left(\frac{\gamma}{2}\right)^2} \qquad (3.5.8)$$

$$\Delta\Omega_s = 2.5 \times 10^{-10}\ I$$

where I is in W/cm^2, N in cm^{-3}, L in cm, δ, $m\Delta\omega$, γ, and $\Delta\Omega_s$ in cm^{-1}.

Example

$$N = 5 \times 10^{17}\ cm^{-3}$$

$$L = 50\ cm$$

$$\delta = 0.12\ cm^{-1}$$

$$\gamma = 0.05\ cm^{-1}*$$

To obtain $\eta_a = 0.2$, the required intensity is $I = 2.4 \times 10^7\ W/cm^2$. For a 100 mJ, 100 nsec long pulse, the corresponding beam parameters are:

$$A = P/I = 0.04\ cm^2$$

$$d = 4A/\pi = 0.23\ cm$$

For the Kerr index, the focusing length and the Stark shift, one finds:

*Estimate

$$n - 1 < 1.4 \times 10^{-8}$$

$$Z_f > 500 \text{ cm}$$

$$\Delta\Omega_s \simeq 0.006 \text{ cm}^{-1} \ll \delta$$

With $\eta_B = 0.27$, $\eta_t = 1$, $\eta_f = 0.5$, the gain (3.5.2) for this example is:

$$g = 0.5 \times 0.2 \times 0.5 \times 1 \times 0.27 \times 2 \times 10^{-19} \times 2 \times 10^{17}/0.04 = 1.4\%$$

If the laser bandwidth would be increased by a factor 16 to a FWHM value of 1.6 cm^{-1}, the intensity required to keep the same absorption efficiency would go up by a factor of four to $I \simeq 10^8 \text{W/cm}^2$. For the same pump energy, this would require $A = 0.01 \text{ cm}^2$. The gain would then also be four times higher, i.e., $g \simeq 6.4\%$, while $Z_f > 250$ cm and $\Delta\Omega_s = 0.024 \text{ cm}^{-1} \ll \delta$.

For Cd the sum of three photons (such that the sum of two photons is two photon resonant) is in the continuum, and attention should be paid to ionization of the atoms in the two-photon excited level. In the absence of radiative trapping for the $2 \rightarrow 1$ transition (see Figure 3.6a), the ionization probability during the lifetime of level 2 must be much less than unity, i.e.,

$$W_i \tau < 1$$

or

$$\sigma_i < \frac{h\nu}{I\tau} \qquad (3.5.9)$$

For the Cd example, with $\tau \simeq 1$ nsec[18] and $I = 10^8 \text{ W/cm}^2$, this requires $\sigma_i < 5 \times 10^{-18} \text{ cm}^2$. Since typically[19]

$$10^{-20} \text{ cm}^2 < \sigma_i < 10^{-17} \text{ cm}^2$$

the effect of ionization would most likely be small. However, because of the relatively high densities in level 1, trapping will occur. As a result, the radiative lifetime has to be replaced by an effective lifetime τ/g, where:[10]

$$g = \frac{1.115}{(\pi\, k_p\, R)^{\frac{3}{2}}} \qquad (3.5.10)$$

with

$$k_p = \frac{\lambda^2\,(N_1 - N_2)}{4\pi^2}\ \frac{g_1}{g_2}\ \frac{1}{\gamma\tau}$$

g_1 and g_2 are degeneracy factors, and γ is the pressure broadened linewidth of the $2 \rightarrow 1$ transition (in radians). For the Cd example, λ = 480 nm, $g_1 = g_2$, $\tau \simeq 10^{-9}$ sec and $\gamma \simeq 1\ cm^{-1}$* (due to the buffer gas). This yields:

$$k_p = 2 \times 10^{-12}\,(N_1 - N_2)$$

$$g = \frac{4.5 \times 10^5}{(N_1 - N_2)^{\frac{3}{2}}\ R^{\frac{3}{2}}}$$

For a beam radius of .16 cm ($A = 10^{-2}\ cm^2$):

$$g = \frac{1.9 \times 10^6}{(N_1 - N_2)^{\frac{3}{2}}}$$

The population difference $N_1 - N_2$ varies in time, according to the rate equations (see Figure 3.7).

$$\dot{N}_2 = R_p - W_i\, N_2 - g\, N_2/\tau$$

$$\dot{N}_1 = g\, N_2/\tau$$

where $R_p = NW^{(2)}$. These equations can be solved numerically for various values for W_i, or, for a given intensity, for $\sigma_i = W_i h\nu/I$. In the case of Cd, level 1 is actually a set of 3 levels, with different lifetimes for each transition, but in this calculation we will use an average lifetime of 1 nsec for the multiplet. Figure 3.8 shows some results, for $I = 10^8\ W/cm^2$. For cross sections below $10^{-19}\ cm^2$, the effect of ionization on the population N_1 is small. For a cross section of $10^{-18}\ cm^2$, however, ionization results

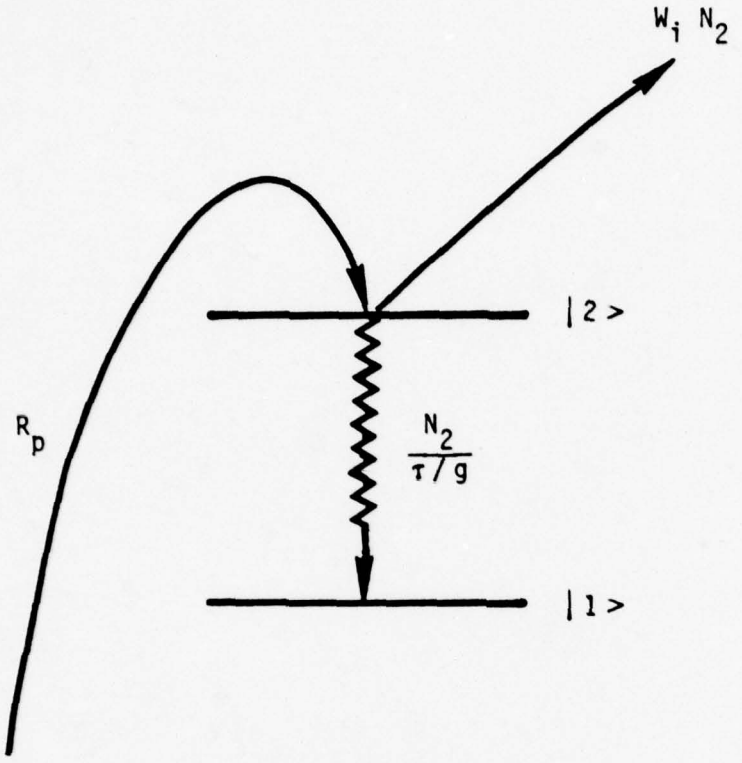

Figure 3.7 Radiative Trapping and Photoionization Losses in Two-Photon Pumping

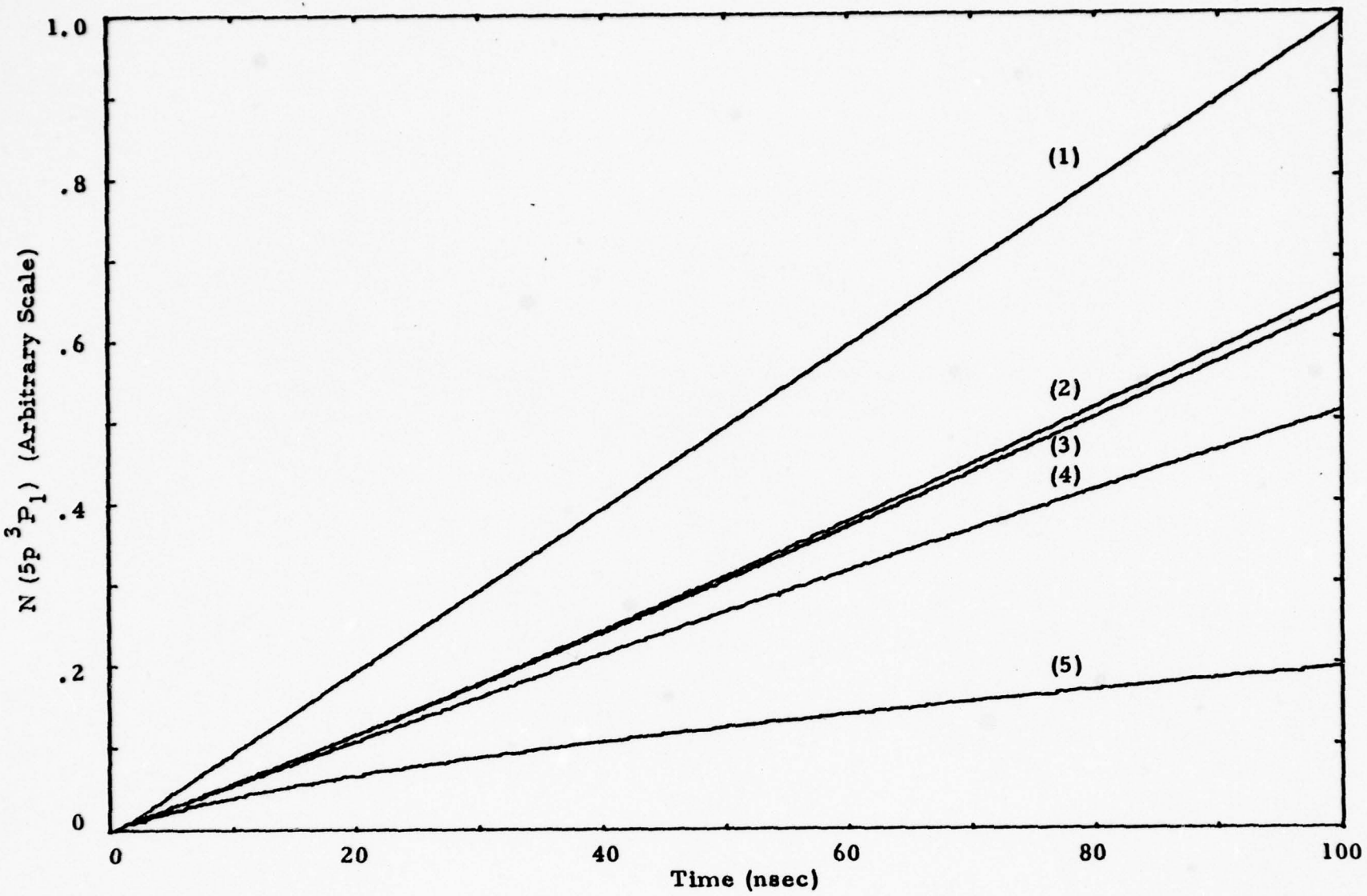

Figure 3.8 Effect of Radiative Trapping and Photoionization on the Population Build-Up in the $5p^3P_1$ Level of Cd
(1) No trapping, $\sigma_i = 0$; (2) → (5) With Trapping, $\sigma_i = 0, 10^{-20}, 10^{-19}, 10^{-18}$ cm^2

in a factor of five decrease for the population of level 1. This would result in a corresponding decrease in the gain.

3.6 Conclusions of Excitation Method Study

a. Metal vapor discharge lamps

The gains obtainable with this method are very small. In addition, the spatial inhomogeneity of the excitation would make the interpretation of experimental data very difficult.

b. Flashlamp pumping

Gains up to 2% are predicted for CdHg for a 10J, 1.5 μsec pulse. However, there may be considerable problems associated with having a high temperature laser tube in an elliptical cavity together with a flashlamp, which normally requires water cooling.

c. Single-photon laser pumping

For a 10 mJ doubled dye-laser pulse at 326.1 nm, gains on the order of 10% are predicted for CdHg. Except for the fact that different dyes may be needed for the excitation of different atoms, the method is general.

d. Two-photon laser pumping

For a 100 mJ dye laser pulse at 388.5 nm, gains of about 6% are predicted for CdHg, if photoionization losses are low. Advantages of this method are that no doubling crystal is required, there are no focusing problems, and the method is general. However, for elements like Cd there are considerable uncertainties about the actual excited state populations that might be obtained because of the possibility of photoionization. As a result, it would be risky to select this method as an only choice. Since the setup for this scheme is identical to the one needed for single-photon pumping, however, it would be a simple matter to

compare the efficiency of both methods experimentally for each particular case.

As a result of this study, it was decided to use single-photon pumping by a tunable laser to excite the Cd atoms. Detailes of the experimental apparatus are discussed in Section 5.

4.0 KINETIC MODELING OF THE CdHg SYSTEM

In order to determine the optimal gas mixtures and the $CdHg^*$ population density which results from optical excitation of Cd, the system was modeled by a set of coupled rate equations. Processes and rates which were included are summarized in Table 4.1. These are illustrated diagramatically in Figure 4.1.

Table 4.1 Kinetics of CdHg with Optical Excitation of Cd ($5\ ^3P_1$)

	Reaction			Rate	Source
1.	$Cd + h\nu$	→	Cd^*	$\frac{\int I(\nu,t)\sigma(\nu,\nu_0)d\nu}{h\nu_0}$	-
2.	$Cd^* + Hg + M$	→	$CdHg^*$	$6 \times 10^{-31}\ cm^6\text{-}s^{-1}$	Ref. 6
3.	$CdHg^*$	→	$Cd + Hg + h\nu$	$2.1 \times 10^5\ s^{-1}$	NRTC
4.	$CdHg^+ + Cd + M$	→	$Cd_2Hg + M$		-
5.	$CdHg^* + Hg + M$	→	$CdHg_2 + M$		-
6.	$CdHg^* + CdHg^*$	→	Products	$2.5 \times 10^{-11}\ cm^3\text{-}s^{-1}$	Ref. 6
7.	$Cd^* + Cd + M$	→	$Cd_2^* + M$	$3 \times 10^{-31}\ cm^6\text{-}s^{-1}$	Ref. 6
8.	Cd_2^*	→	$Cd + Cd + h\nu$	$3.3 \times 10^5\ s^{-1}$	Ref. 6

In this model, the $5\ ^3P_1$ level of cadmium (Cd^*) is pumped optically at a rate

$$k_1(t) = \frac{\int I(\nu,t)\sigma(\nu,\nu_0)d\nu}{h\nu_0} \qquad (4.1.1)$$

Here $I(\nu,t)$ is the pump source intensity as a function of frequency and time, and $\sigma(\nu,\nu_0)$ is the atomic absorption cross section centered at frequency ν_0.

Three-body collisions between Cd^*, Hg, and a buffer gas, such as Ar, form the excimer $CdHg^*$. There are indications that two excimer levels in CdHg are responsible for the blue emission.[3] For the present purposes, these two levels are grouped and treated as one excimer state. A model incorporating two levels is discussed later in conjunction with experimental results from this work.

Removal of $CdHg^*$ can occur from radiative decay, biexcimer quenching, or three-body quenching with Cd or Hg. Loss of excited cadmium atoms by radiation is neglected. Although the Cd^* radiative lifetime is about 3 μs, calculations show that with Cd densities on the order of 10^{17} cm^{-3}, radiative trapping causes the effective lifetime to be much longer. Dimerization of Cd is included as a loss mechanism for Cd^*.

On the basis of the reactions listed in Table 4.1, it is possible to estimate optimal number densities for Cd and Hg. In order to maximize formation of $CdHg^*$ relative to Cd_2^*, it is required that

$$k_2 [Hg] > k_7 [Cd]. \tag{4.1.2}$$

A ratio of 10:1 for formation of $CdHg^*$ relative to Cd_2^* is probably reasonable, so

$$k_2 [Hg] = 10\, k_7 [Cd]. \tag{4.1.3}$$

Thus the ratio of [Hg] to [Cd] should be

$$[Hg]/[Cd] = 10\, k_7/k_2 = 5. \tag{4.1.4}$$

Because of the spectral width of the pump pulse, Cd number densities on the order of 4×10^{17} cm^{-3} are needed for efficient absorption of the pump radiation. This indicates that Hg number densities on the order of 2×10^{18} cm^{-3} are required. It is not advisable to have Hg number densities much higher than this value because of possible absorption at 326 nm by ground state Hg_2. For this reason, argon is used to increase the three-body formation rate of CdHg. The Ar density should be limited to about 8×10^{18} cm^{-3} to avoid excess pressure when the quartz cell is heated.

Differential rate equations for the system of equations listed in Table 4.1 were derived and integrated as a function of time to predict number densities for Cd^*, $CdHg^*$, and Cd_2^*. Integration was performed numerically using a fourth-order Runge-Kutta method.

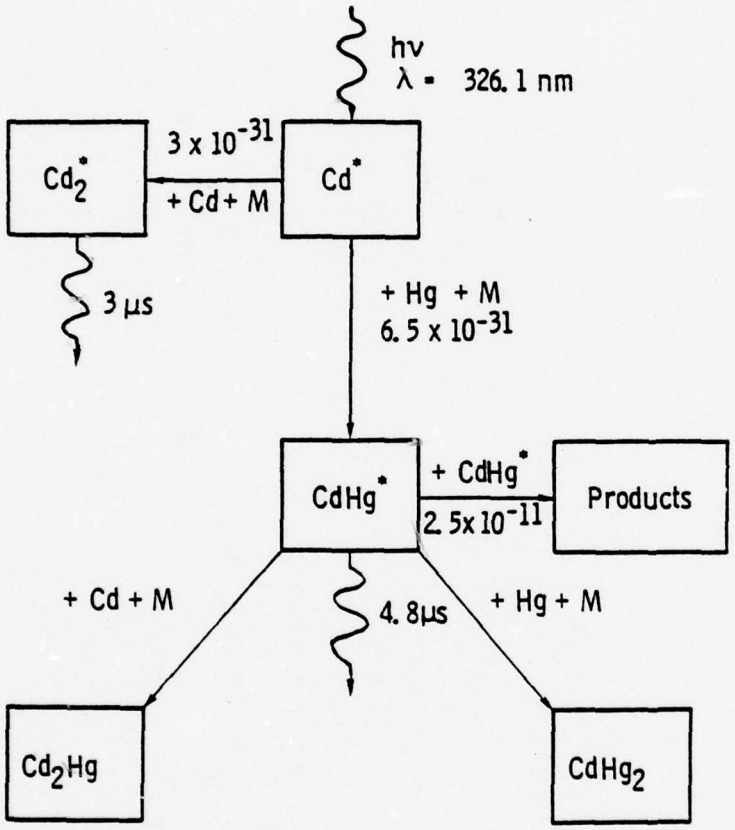

Figure 4.1 CdHg Kinetics with Optical Excitation at 326.1 nm

The optical excitation pulse was modeled as a triangular waveform having a FWHM of about one microsecond. A pump energy of 0.25 mJ was assumed to be deposited in a volume of 0.5 cm^3.

These conditions closely approximate the experimental conditions when the 50 cm long metal vapor cell, described in Section 5, is pumped with a frequency doubled, Chromatix CMX-4 dye laser. Figure 4.2 shows the results of these calculations. It is seen that Cd^* rapidly forms $CdHg^*$ and that $CdHg^*$ densities are about a factor of ten greater than Cd_2^* densities. At these low excited state densities, biexcimer quenching processes (Step 6 in Table 4.1) are unimportant, although they were included in the calculations. Since rate constants for the trimer formation reactions (Steps 4 and 5) are not known, it is assumed at this time that these processes are negligible. A value of $k = 10^{-33}$ cm^6 $-s^{-1}$ was assumed for each of these steps.

Another calculation was done to estimate the kinetic efficiency for formation of $CdHg^*$ from Cd^*. Here an initial Cd^* density of 5×10^{14} cm^{-3} was assumed, and the equations were integrated to find the maximum $CdHg^*$ density. These results are shown in Figure 4.3. Formation efficiencies exceeding 80% are predicted, assuming quenching processes are small. Actually, since the value for K_3 (radiative decay of $CdHg^*$) is taken from fluorescence measurements obtained under experimental conditions similar to those of the gain studies, this value includes any quenching which may be present. Thus, it is proper to exclude additional quenching for the purposes of these calculations.

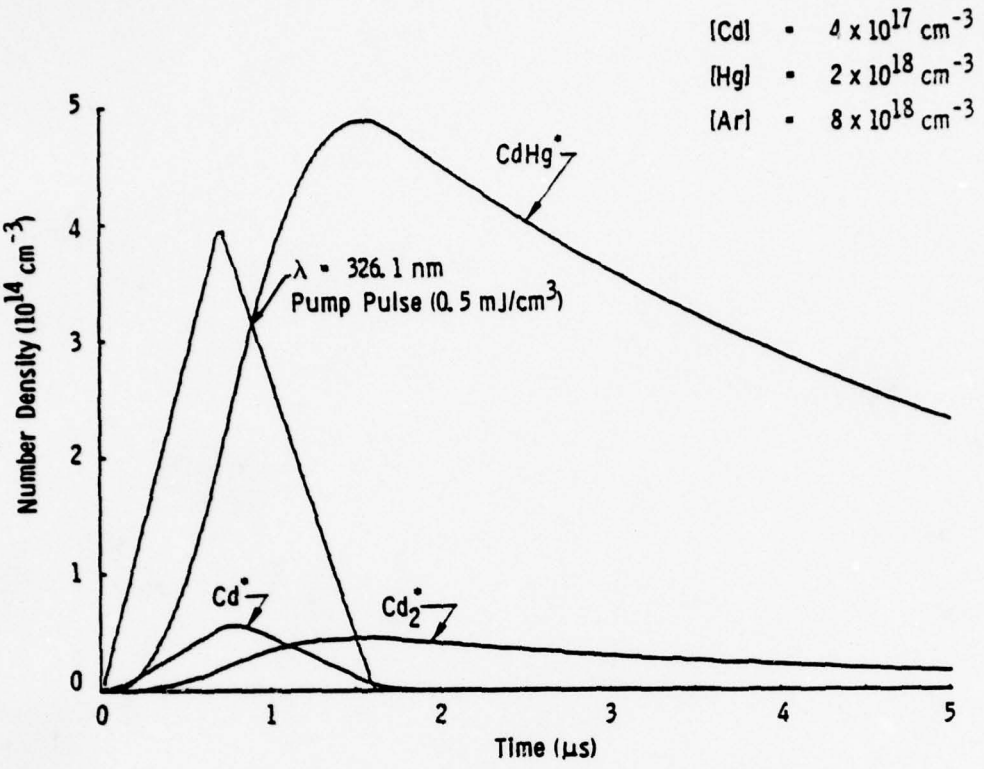

Figure 4.2 CdHg Excimer Kinetics

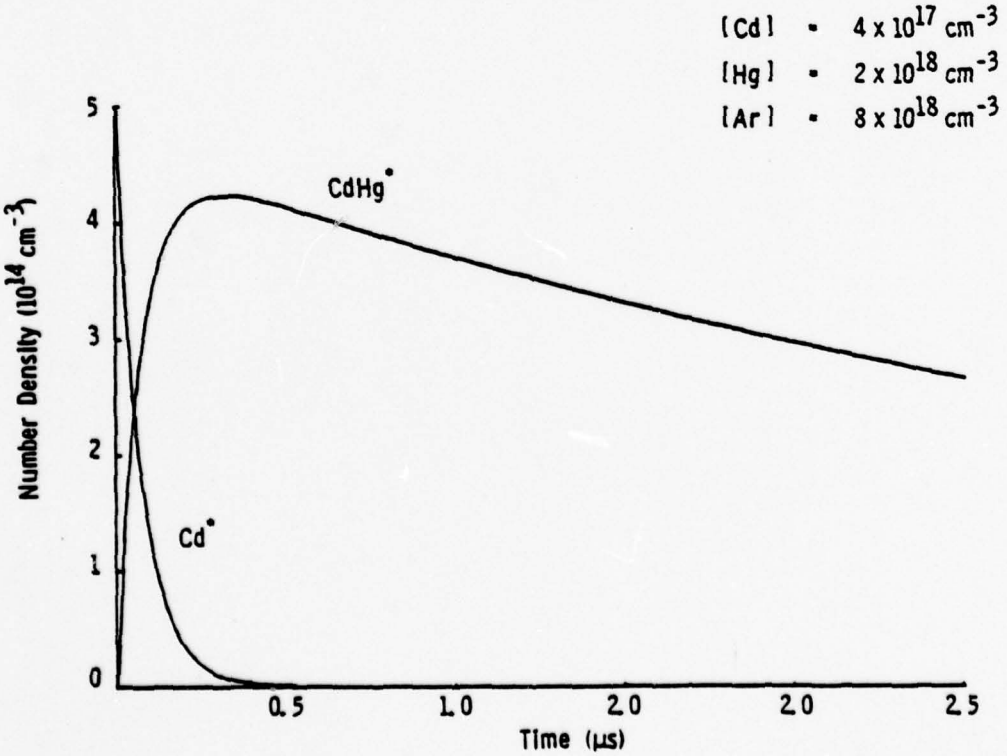

Figure 4.3 Formation Efficiency of $CdHg^*$

5.0 EXPERIMENTAL APPARATUS

5.1 Metal Vapor Cell

A special cell, designed for laser excitation of metal vapors was constructed for these experiments. This is shown in Figure 5.1. The entire heated portion is fabricated from quartz to allow operation at temperatures in excess of 600 C if necessary. Quartz windows for entrance and exit of the laser beams are fused to the body of the cell at Brewster's angle to reduce transmission losses. The windows are heated to the same temperature as the rest of the cell and are isolated from the cooler laboratory atmosphere by a vacuum space. This prevents metal condensation on the windows as well as distortion of the laser beams due to thermal gradients. The cell shown in Figure 5.1 has an optically excited volume which is 1 mm in diameter and 50 cm in length. Special high temperature heating tape is used to achieve the necessary temperatures in the cell, which is contained in an insulating enclosure of fire bricks and Pyrex wool.

Cell temperatures are measured with six chromel-alumel thermocouples held against the quartz surface by asbestos tape at locations shown in Figure 5.2. Cadmium densities are regulated by controlling the temperature of a side arm separately from the main cell temperature. Cadmium partial pressures are found either by using a graph[20] of pressure versus temperature or an empirical relationship between pressure and temperature,[21]

$$\log P_{Cd} = 12.467 - \frac{5910}{T} - 1.234 \log T - 0.000156\, T \qquad (5.1.1)$$

In the above equation, P_{Cd} is given in Torr and T is the side arm temperature expressed in degrees Kelvin. The cadmium number density in the upper cell is then found using the ideal gas law

$$n_{Cd} = \frac{P_{Cd}}{k\, T_{cell}} \qquad (5.1.2)$$

If P_{Cd} is measured in Torr, n_{Cd} in cm^{-3}, and T_{cell} in degrees Kelvin, then the appropriate value of the gas constant is $k = 1.04 \times 10^{-19}$. Under certain conditions, the formation of a cadmium-mercury amalgam can strongly influence the cadmium vapor pressure.[6] This effect is most important at lower cell temperatures, and it becomes negligible at temperatures typically used in the NRTC experiments.

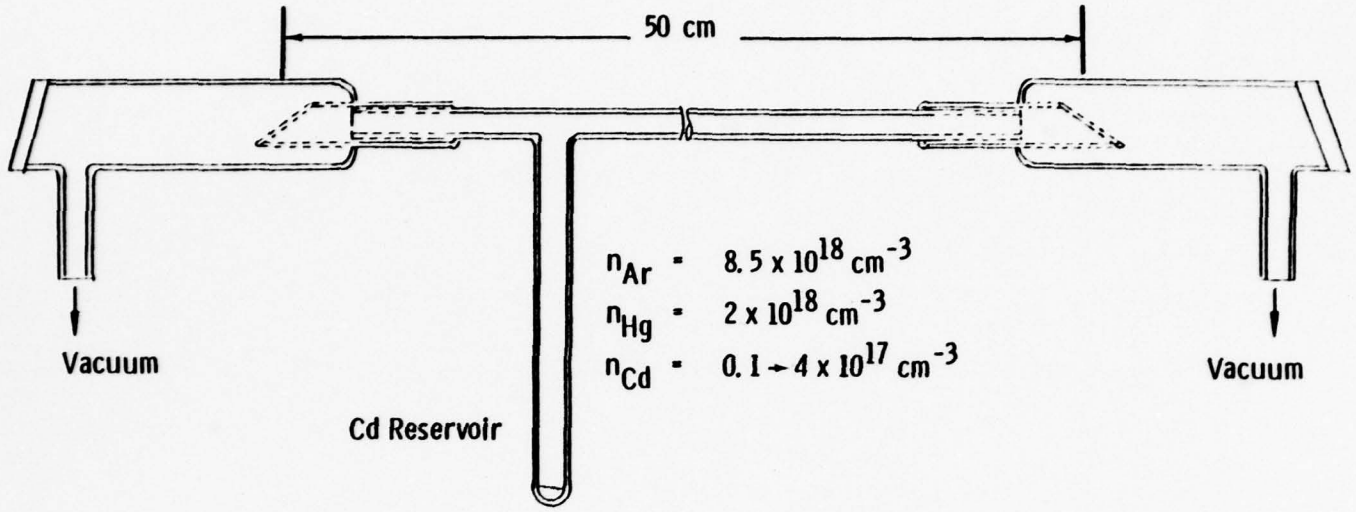

Figure 5.1 CdHg Metal Vapor Cell

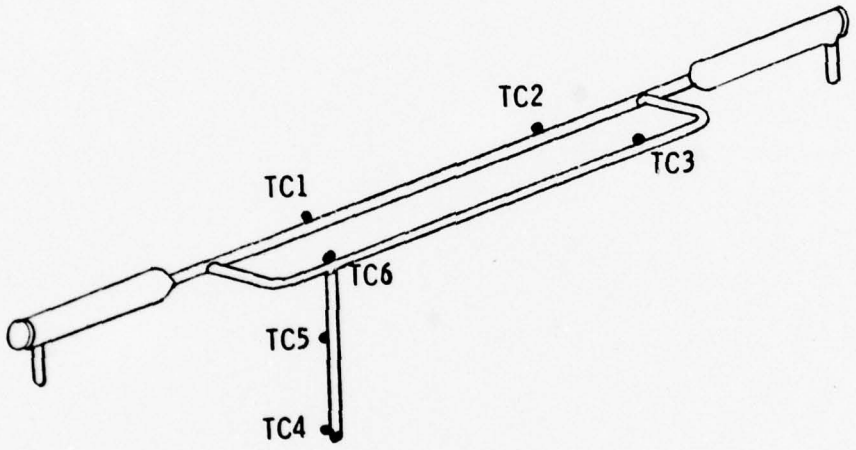

Figure 5.2 Thermocouple Locations on CdHg Cell

5.2 Processing the Metal Vapor Cell

Since the boiling point of mercury is only 370 C, it is necessary to distill the desired amount of Hg into the cell prior to sealing it. When introducing metals into the cell, cleanliness is extremely important. For these experiments, a careful distillation procedure was used. First, the desired amounts of mercury and cadmium were weighed on an analytical balance. Since the total volume of the cell is 54 cm^3, 36 mg of Hg are required for a number density of 2×10^{18} cm^{-3}. A total of 40 mg of Hg was used to allow for a small loss in transferring the metal. It was desired to have an excess of Cd, so 40 mg of this metal was also weighed out. The distillation procedure used is described in the following paragraphs.

A Pyrex tube was fabricated as shown in Figure 5.3. Attached to this tube was a quartz ampule to contain the Cd and Hg. This was heated with heating tapes and pumped with a liquid nitrogen trapped diffusion pump to a pressure on the order of 1×10^{-6} Torr. The tube was then cooled and pressurized with high purity argon. Using a torch, point A was opened and the metals introduced to point C. Point B was then sealed with a torch after which point C was cooled in liquid nitrogen. At this time, the tube was reevacuated, and the U-trap at point E was cooled with liquid nitrogen. Point C was then warmed and a low temperature torch was used to gently drive the metals into the U-tube at point E. With the tube under vacuum, point D and then point F were sealed. The U-tube was then warmed and the metals driven into the ampule, after which point G was sealed. The ampule was then attached to the high temperature cell. During the transfer process, the mercury transferred first at lower temperatures and did not appear to leave any visible residue. Higher temperatures were required to transport the Cd, and a small residue was left behind at point C. After the ampule was attached to the cell, the whole apparatus was baked and pumped to about 1×10^{-6} Torr. Following the baking and pumping, 260 Torr of purified argon was added to the cell, which was then sealed off. Under these conditions, the estimated number densities in the cell are:

Ar: 8.5×10^{18} cm^{-3}

Hg: 2×10^{18} cm^{-3}

Cd: $0.1\text{-}4 \times 10^{17}$ cm^{-2}, controlled by side-arm temperature.

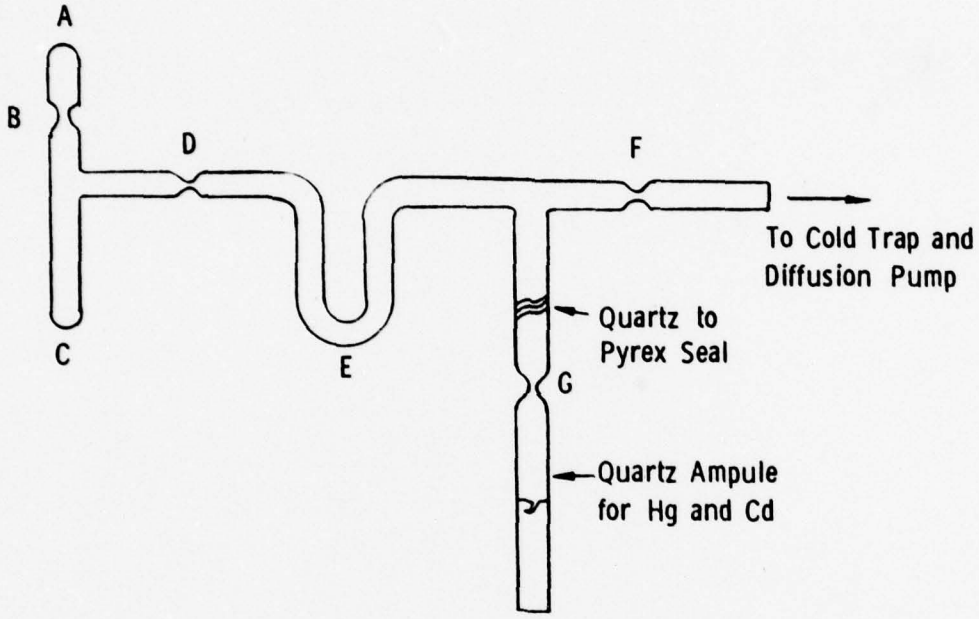

Figure 5.3 System for Filling Ampule with Hg and Cd

An indication of cell cleanliness is the lack of any visible fluorescence excited by either an argon-ion laser or a uv laser at wavelengths near, but not on, the Cd absorption line.

5.3 Gain/Absorption Probe

A Coherent Radiation Model 54 argon-ion laser is used as a probe for either gain or absorption in the CdHg blue fluorescence band. This laser produces continuous output with powers up to several hundred milliwatts at several wavelengths in the CdHg spectrum. These are listed in Table 5.1 below:

Table 5.1 Argon-Ion Laser Wavelengths

λ (nm)
457.9
472.7
476.5
488.0
496.5
501.7
514.5

Since the output of the probe laser had about 4% amplitude noise at frequencies between 0.1 to 1 MHz, a differential detection method, described in Section 5.4 was used. This noise varied with probe wavelength. Lowest noise occurred at 457.9 and 496.5 nm, while the highest noise was at 488 nm.

5.4 Detection System and Electronics

In order to achieve high detection sensitivity, a special differential amplifier was designed and built. A schematic diagram of this device is shown in Figure 5.4. Two silicon photodiodes are used to observe the probe beam and a portion of the argon-ion laser beam which has bypassed the metal vapor cell (reference beam). These photodiodes are reverse biased and their output currents are summed at the inverting input of a high speed operational amplifier (LH0032). The circuit is designed so that with equal light intensity on each photodiode, the resulting currents cancel and there is no output. Small changes in one of the light beams create an imbalance which is amplified, whereas

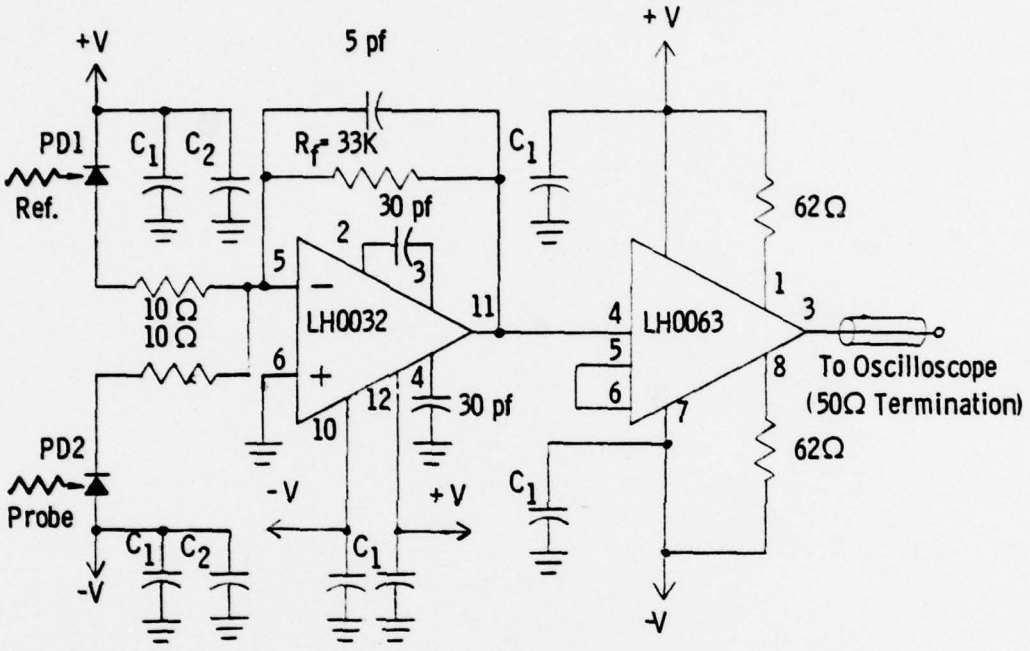

Figure 5.4 Differential Amplifier for Gain/Absorption Measurements

intensity variations common to both laser beams tend to cancel. This is important, since the argon-ion laser has up to 4% amplitude noise. The relation between the output voltage and input current depends on the feedback resistor, R_f, in the equation

$$V_{out} = - R_f I_{in} \qquad (5.4.1)$$

The final amplifier shown in Figure 5.4 is a high speed, unity gain buffer (LH0063) which is able to drive a 50 ohm transmission line leading to a storage oscilloscope.

In using the circuit shown in Figure 5.4 to find a fractional change in the probe beam intensity, it is necessary to compare a high speed pulse signal (the gain or absorption change) to the dc signal level of the probe beam when it strikes only the probe photodiode. Thus it is necessary to know where the high frequency response of the circuit begins to roll off. To determine this, a 7 ns pulse from a frequency-doubled Nd:YAG laser was allowed to strike the probe photodiode. The resulting signal showed a 0.32 μs exponential decay, indicating the circuit transfer function is that of an RC low pass filter having a time constant of T = 0.32 μs.

$$g(s) = \frac{1}{s + \frac{1}{T}} \qquad (5.4.2)$$

Pulses similar to those observed experimentally (see Figure 6.6) were modeled using the transfer function in Equation (5.4.2). It was found that some degradation in pulse rise time occurs, and that the peak value is attenuated about 15%. Results reported here are not corrected for this attenuation, so actual absorption values may be slightly greater than those stated.

In addition to the Nd:YAG laser measurement of circuit pulse response, the 1 μs wide pulse from the CMX-4 dye laser (see Section 5.5) was also measured using the circuit in Figure 5.4. The resulting pulse shape was compared to that observed using a fast planar photodiode. A slight degradation in rise time was observed, but the decay time and pulsewidth were not affected.

5.5 326.1 nm Excitation Source

Several different methods have been used to generate the 326.1 nm radiation needed for excitation of the cadmium atoms. For low pulse energies, a Chromatix CMX-4, equipped with intracavity frequency doubling crystals, is used. Approximately 0.3 mJ is generated at 326.1 nm in a 1 μs FWHM pulse, having a spectral width of about 5.5 cm^{-1}.

To obtain higher energies at 326.1 nm, a coaxial flashlamp pumped dye laser is used to generate output at 652.2 nm which is frequency-doubled by a KDP crystal. Approximately 120 mJ is produced at the red wavelength, leading to second harmonic energies up to 5 mJ per pulse.

A negative branch unstable resonator[22] is used to improve the spatial mode of the coaxial dye laser. Since this approach makes frequency tuning of the dye laser difficult, the CMX-4 dye laser is used to injection lock[23] the higher power dye laser. This technique works very well, concentrating nearly all of the coaxial dye laser energy into a linewidth determined by the width of the CMX-4 output ($\approx$3 cm^{-1}). From Equation (4.4.4), the necessary detuning of the uv laser from the Cd absorption line center is estimated to be about 14 cm^{-1}. This detuning is greater than the laser linewidth and in practice, the optimum pump laser wavelength is determined experimentally by measuring the transmitted intensity through the heated metal vapor cell.

5.6 Experimental Facility

Figure 5.5 is a diagram showing the relationship of the various experimental elements of the CdHg facility. The uv beam from the CMX-4 laser is condensed to about 1 mm diameter by telescope 1 and directed through the metal vapor cell. Photodiodes PD_1 and PD_2 monitor input and transmitted intensities with the laser tuned to the Cd atomic resonance and just off-resonance in order to determine the fraction of energy absorbed in the cell.

Figure 5.6 shows the arrangement incorporating the Phase-R coaxial flashlamp dye laser used to obtain higher pulse energies. Output from the CMX-4 is mode-matched with a telescope and coupled into the Phase-R through a 45^{o} mirror which transmits about 5% at 652 nm. The injection-locked dye output is then frequency-doubled by a KDP crystal to obtain up to 5 mJ at 326 nm.

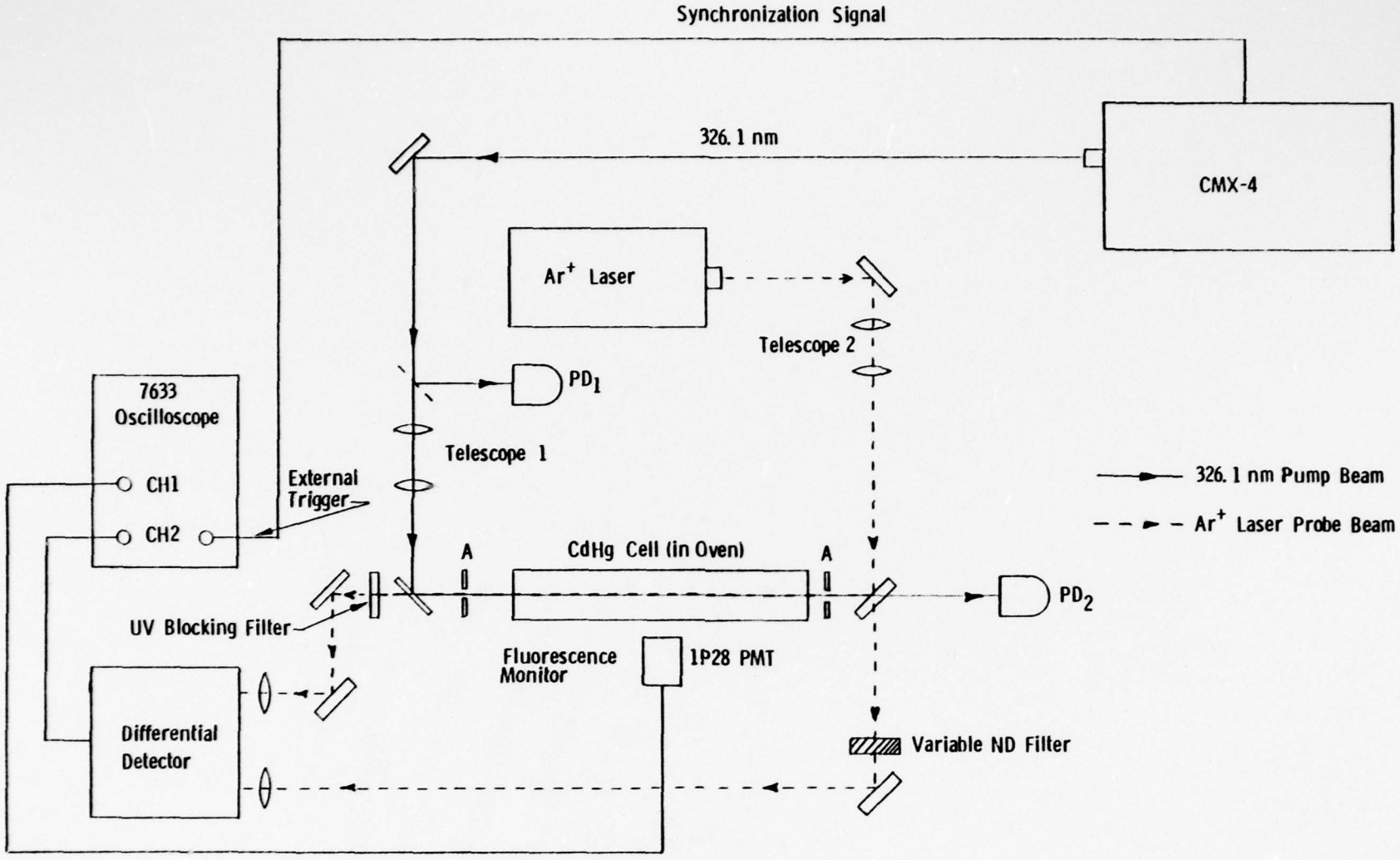

Figure 5.5 Experimental Facility for CdHg Gain/Absorption Experiments

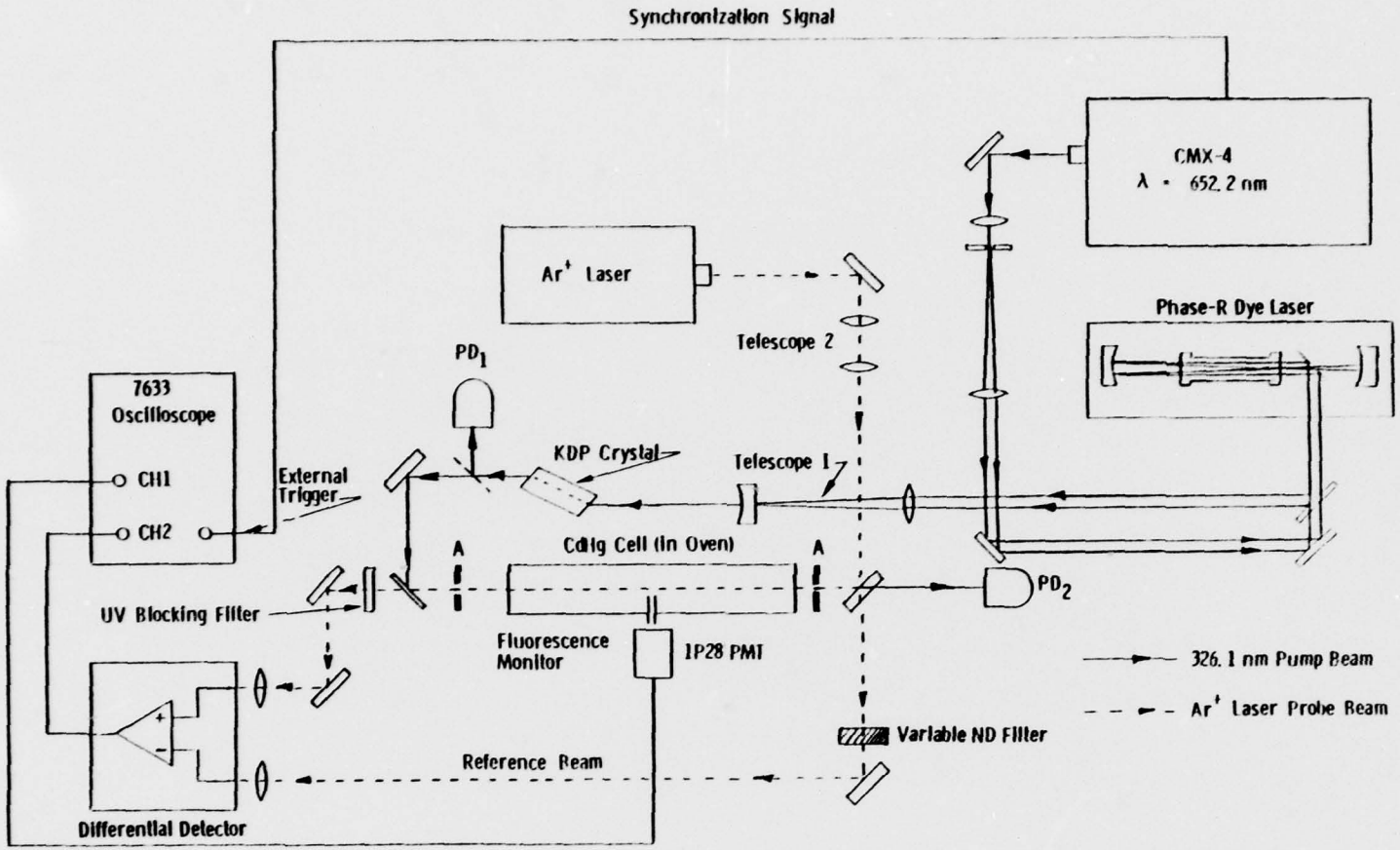

Figure 5.6 Experimental Facility for CdHg Gain/Absorption Measurements at Higher Pump Energies

The argon-ion laser probe beam is condensed by telescope 2 and a portion is directed through the cell. Apertures, A, are used to spatially overlap the uv pump beam and the probe beam. The probe beam and a portion bypassing the cell (reference beam) are loosely focused on the two photodiodes of the differential amplifier described in Section 5.4. A variable neutral density filter is placed in the reference beam to equalize the light intensity on the two diodes when no gain or absorption is present. When this is done, the high frequency amplitude noise on the argon-ion laser beam is reduced about an order of magnitude because of cancellation by the two diodes. A 1P28 photomultiplier tube views the CdHg fluorescence through the side of the cell and this signal can also be displayed on the oscilloscope for comparison with any gain or absorption signal. This photomultiplier is used with a special base having capacitors across the last dynode stages to improve the response to pulsed signals.

6.0 EXPERIMENTAL RESULTS

6.1 Fluorescence Measurements

With the metal vapor cell containing a mixture of $n_{Ar} = 8.5 \times 10^{18}$ cm^{-3}, $n_{Hg} = 2 \times 10^{18}$ cm^{-3}, and $n_{Cd} = 0.1$ to 4×10^{17} cm^{-3} as described in Section 5, fluorescence measurements of the blue CdHg emission were made. With the exception of data presented in Figure 6.4, the CMX-4 dye laser described in Section 5.5 was used for all measurements in this section.

First, a fluorescence spectrum was obtained. For this purpose, a 1/4 meter grating spectrograph equipped with 1P28 photomultiplier was used. Corrections for detection system response were applied to the spectrum which is shown in Figure 6.1, along with positions of argon-ion probe laser lines used at NRTC for absorption measurements. The spectrum shows several important features. First, the broad continuous emission matches previously published spectra of CdHg;[3] however, it has a stronger red wing than spectra of Cd_2^* obtained by Drullinger and Stock.[24] The blue emission is present only when the pump laser is tuned to the Cd atomic resonance. No fluorescence is observed at other wavelengths, indicating the cell is relatively free of impurities. The fluorescence also goes away when the cell is cooled below 300 C, at which point the Cd vapor pressure is less than 0.1 Torr. These observations confirm that CdHg is the emitting species for the blue fluorescence. Emission at 335 nm due to Hg_2 excimers and at 253.7 nm due to atomic Hg was not observed, indicating excited mercury states do not play an important role in the kinetics of these experiments.

Measurements of the fluorescence time history were obtained by viewing the side of the metal vapor cell with a 1P28 photomultiplier tube. Corning CS3-75 and CS4-72 filters were used to eliminate any scattered uv pump light and stray light outside the fluorescence spectrum. Figure 6.2 shows the temporal relationship between the uv pump pulse from the CMX-4 and the CdHg fluorescence. Figure 6.3 shows the fluorescence signal in more detail. The experimental conditions for Figure 6.3 are shown in Table 6.1.

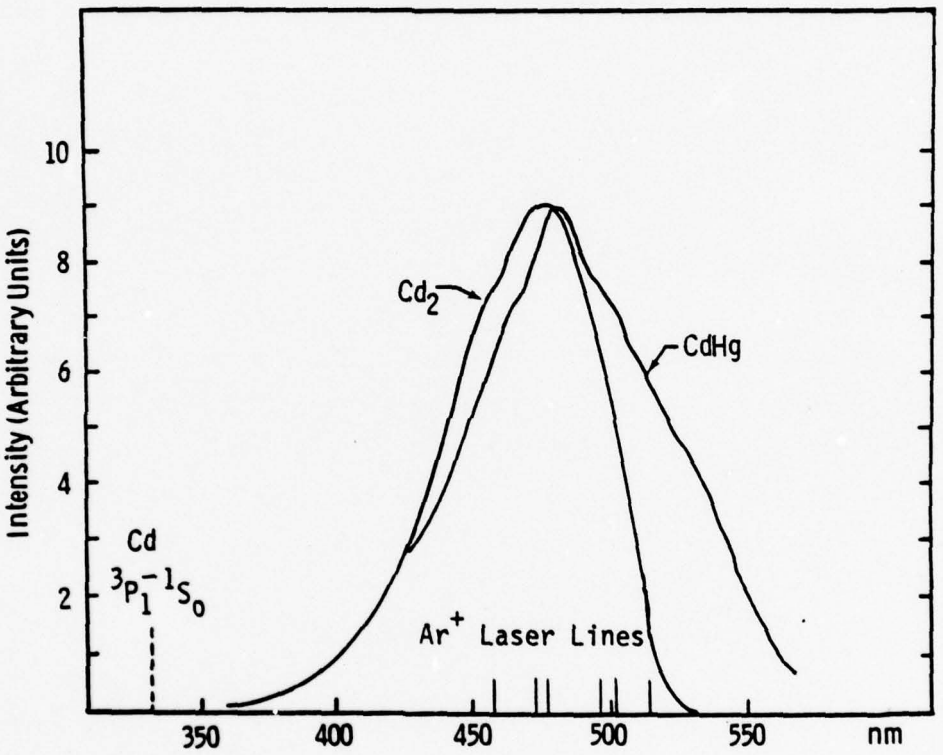

Figure 6.1 Cd_2 and CdHg Fluorescence Spectra (Cd_2 Spectrum from Drullinger and Stock, Ref. 29)

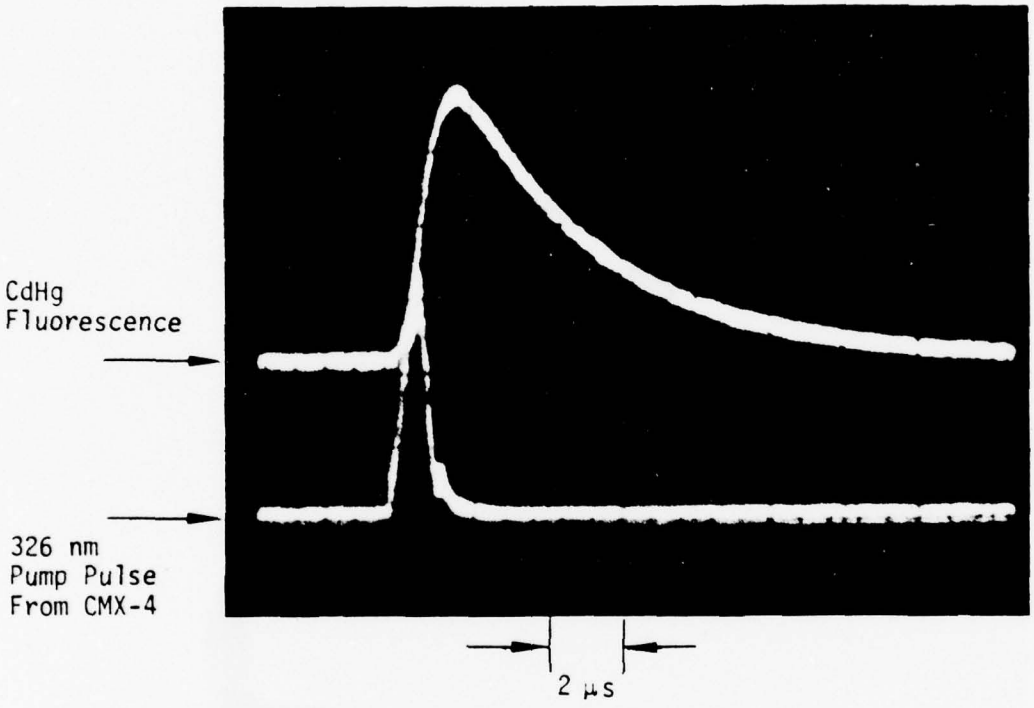

Figure 6.2 CdHg Fluorescence and 326.1 nm Excitation Pulse

(a)

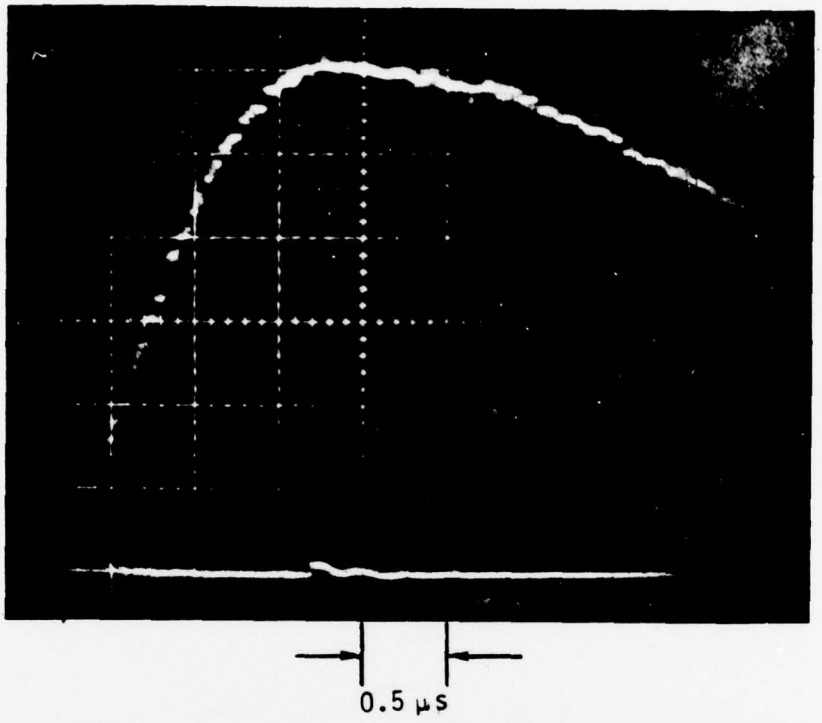

(b)

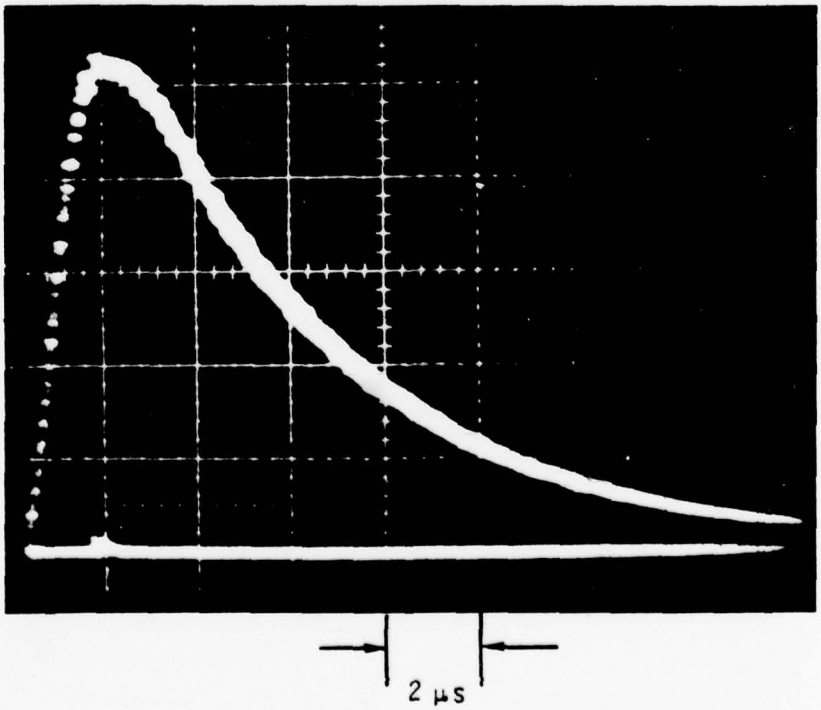

Figure 6.3 CdHg Fluorescence

Table 6.1 Typical Experimental Conditions for Fluorescence Measurements

n_{Ar} =	8.5×10^{18} cm^{-3}	n_{Cd} =	7.2×10^{16} cm^{-3}
n_{HG} =	2×10^{18} cm^{-3}	T_{cell} =	836 K

Similar data were obtained with the cell temperature held constant (near 830 ±5 K) and varying n_{Cd} between 1.0×10^{16} cm^{-3} and 7.2×10^{16} cm^{-3}. Also, data in which n_{Cd} is held constant (near $1.2 \pm 0.13 \times 10^{17}$ cm^{-3}) and T_{cell} is varied between 716 K and 967 K were obtained. In all these experiments, the exponential decay time is nearly the same,

$$\tau_{decay} = 4.8 \pm 0.25\ \mu s, \qquad (6.1.1)$$

and shows no correlation with either cell temperature or cadmium number density. This decay rate represents the combined loss processes due to radiative decay of CdHg along with any quenching processes present, and is slightly longer than either of the two values stated by McGeoch, et al[3] (2.8 μs and 4.0 μs).

When fluorescence decay time is measured as a function of 326.1 nm excitation energy, an inverse relationship is found. At low pump energies, a value of 4.8 μs is observed; however, as the pump energy increases to several millijoules, the decay time shortens, and approaches 2.7 μs. This data is plotted in Figure 6.4, which shows the reciprocal of decay time (decay frequency) as a function of pump energy. A pump energy-dependent fluorescence decay time can be explained by the kinetics scheme shown in Figure 6.5. Two CdHg excimer levels, each with a different decay time, are included. If the three-body formation of $CdHg^*$ has a high branching ratio to the longer lifetime state ($CdHg^*$ (a)), then at low excitation energies a 4.8 μs decay time is observed. At higher pump energies, the excimer density increases and biexcimer collisions transfer the population to the shorter lifetime state ($CdHg^*$(b)). At sufficiently high pump energies this transfer is rapid enough to depopulate the a state so no further decrease is seen in the fluorescence decay. This observation is consistent with the conclusions of McGeoch, et al,[3] who determined a rate constant of 5×10^{-10} cm^3 -s^{-1} for the biexcimer transfer.[6]

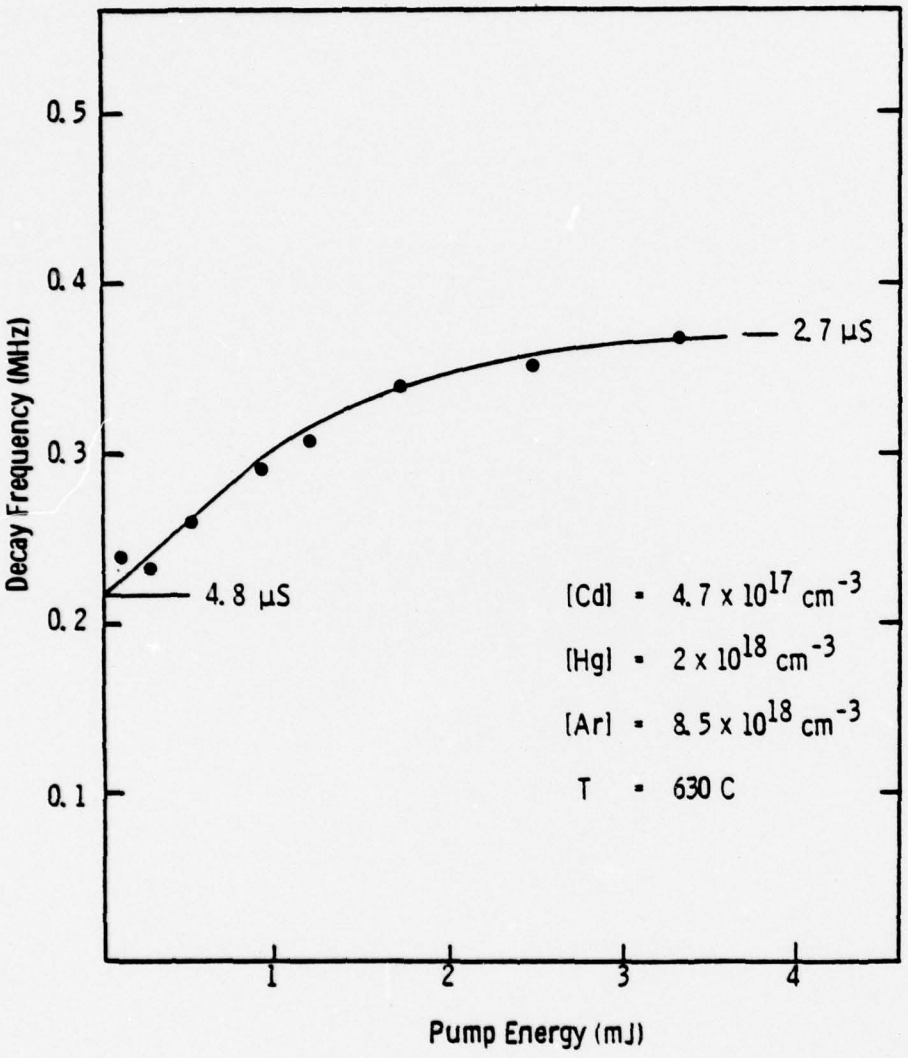

Figure 6.4 $CdHg^*$ Fluorescence Decay vs Excitation Energy

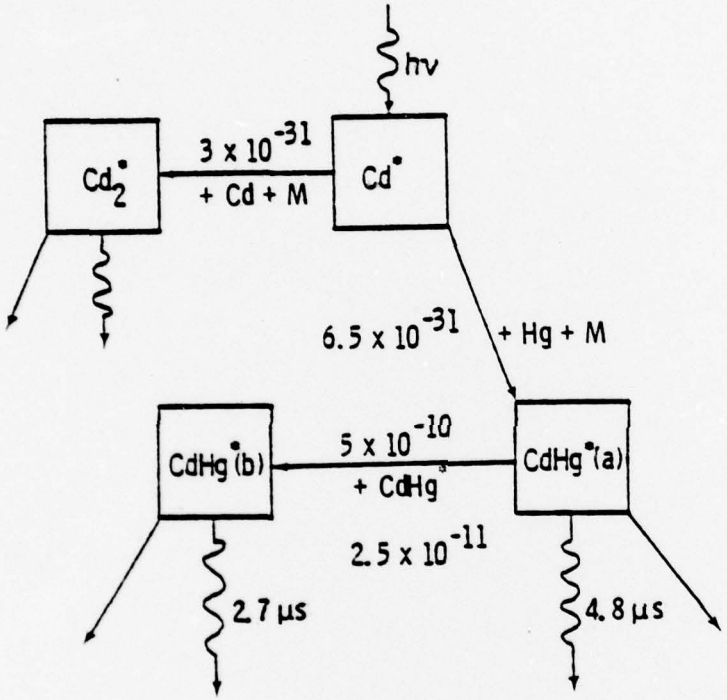

Figure 6.5 CdHg* Kinetics with Optical Excitation at 326 nm

6.2 Gain/Absorption Measurements

Absorption on several lines of the argon-ion laser has been observed. In most of these experiments, the conditions shown in Table 6.2 existed:

Table 6.2 Typical Experimental Conditions for Absorption Measurements

P_{Cd}	=	34 Torr
n_{Cd}	=	3.6×10^{17} cm^{-3}
n_{Hg}	=	2.0×10^{18} cm^{-3}
n_{Ar}	=	8.5×10^{18} cm^{-3}
T_{cell}	=	903 K
$T_{sidearm}$	=	819 K
P_{total}	=	974 Torr

Figure 6.6 shows a typical oscilloscope trace of the absorption signal from the differential amplifier discussed in Section 5.4. For comparison purposes, the fluorescence signal is also displayed. For the case shown in Figure 6.6a, the total dc level from the amplifier with the reference beam blocked was 1.3 V. The magnitude of the absorption signal is about 0.015 V giving a percentage absorption of the probe beam of 1.15% per pass. The measurement shown in Figure 6.6a was performed using the frequency-doubled CMX-4 as the pump. For this case, the pump energy was about 0.15 mJ. The absorption is present only when the pump laser is tuned to the 326.1 nm Cd resonance transition. In Figure 6.6b, the pump energy was 0.75 mJ, obtained from the Phase-R dye laser. Again, the absorption is clearly present. Note the shorter fluorescence decay time which is observed at the higher pump energy.

Data similar to that shown were collected at several wavelengths of the Ar^+ laser and are summarized in Table 6.3. The amount of absorption was found to scale with the 326 nm pump energy, so for comparison purposes, values were normalized to a 1 mJ level. These data are plotted in Figure 6.7 as a function of wavelength.

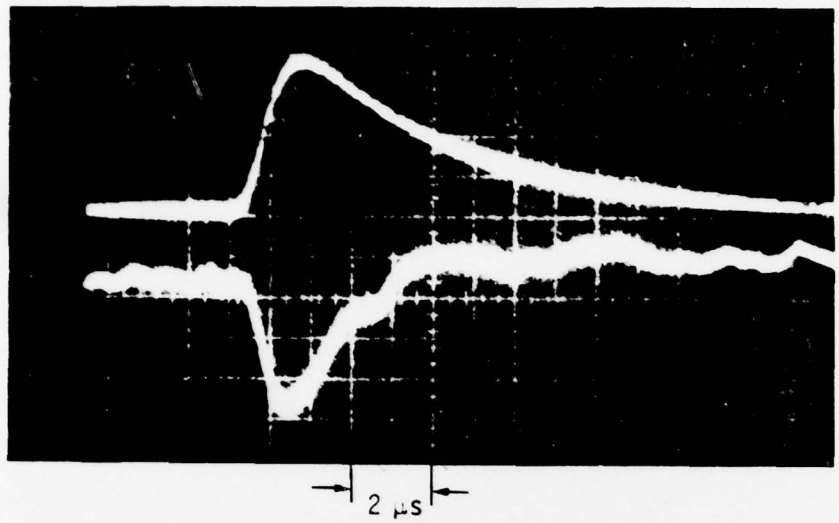

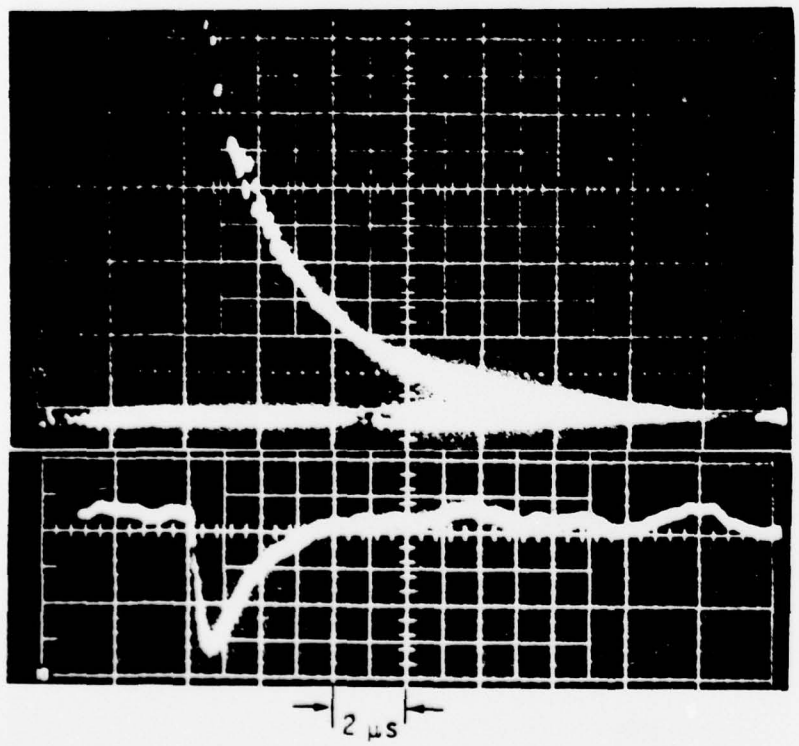

Conditions: $n_{Cd} = 3.6 \times 10^{17}$ cm^{-3}, $n_{Hg} = 2 \times 10^{18}$ cm^{-3}, $n_{Ar} = 8.5 \times 10^{18}$ cm^{-3}, $T = 906$ K, $\lambda_{probe} = 457.9$ nm

Figure 6.6 Absorption in Excited Mixtures of Cd and Hg

Table 6.3 Absorption in Laser Excited CdHg Vapor

Probe Wavelength (nm)	Pump Energy Absorbed (mJ)	Single Pass Absorption (%)	Single Pass Absorption/mJ ($\% \cdot mJ^{-1}$)	Average
457.9	0.34	3.1	9.0	
457.9	0.63	5.3	8.4	8.1
457.9	0.84	5.9	7.0	
472.7	1.1	5.5	5.0	5.0
476.5	0.84	4.0	4.8	5.2
476.5	0.84	4.8	5.7	
496.5	1.26	2.3	1.8	1.8
501.7	0.25	1.1	4.4	
501.7	0.53	1.5	2.8	3.8
501.7	0.63	2.6	4.1	
514.5	0.84	2.4	2.9	2.9

Notes: Absorption Length = 50 cm, Pump Beam Diameter = 0.2 cm,
Cell Temperature = 630 C

Strongest absorption is observed at 457.9 nm, and the effect is seen to decrease as the wavelength of the probe laser increases. The absorption strength appears to be correlated with fluorescence intensity. From the trend in absorption vs wavelength, it appears that the peak values for absorption may occur on the blue wavelength side of the peak value for fluorescence.

In addition to the above data, a measurement at a lower cell temperature was obtained to determine if the absorption is temperature dependent. At a cell temperature of 495 C, absorption is still observed. This point is also shown in Figure 6.7.

A possible error source in the data presented in Table 6.3 involves the spatial overlap of the pump and probe beams. The pump beam had a 2 mm diameter at the

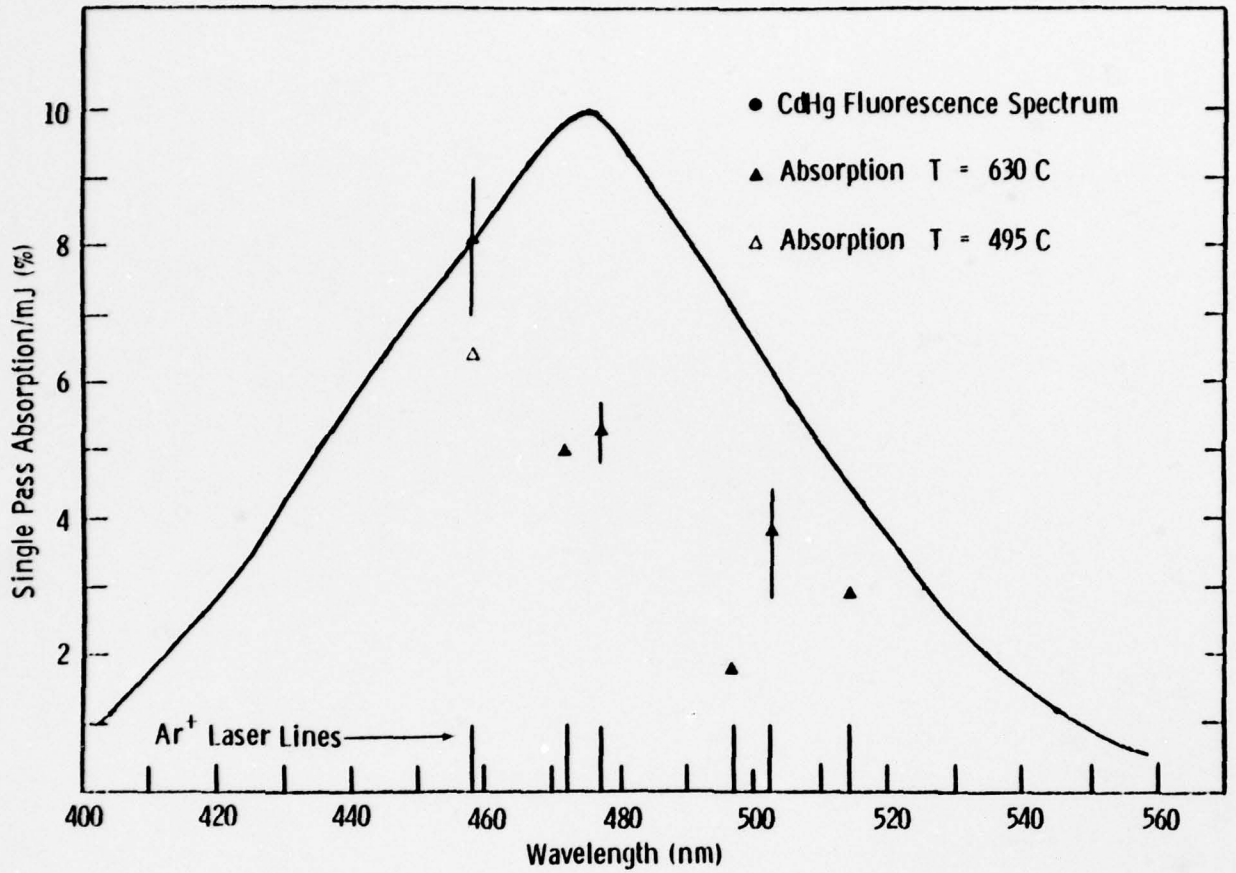

Figure 6.7 Absorption in Laser Excited CdHg Vapor vs. Wavelength

cell entrance window and was focused with a 1 m lens to about a 1 mm diameter at the center of the cell. Since small changes in alignment can occur over extended time periods, the data in Table 6.3 were obtained in a single experiment session. However, careful alignment procedures yielded similar results in all experiment sessions.

6.3 Acoustic and Thermal Effects

When energy is absorbed in a long, narrow volume, as in the case of these experiments, careful attention must be given to possible acoustic effects which could lead to probe beam steering. Any such beam steering could appear as intensity fluctuations which mimic absorption.

An estimate of the thermal loading can be obtained by comparing the pump radiation and fluorescence photon energies. The 326 nm pump photon has 3.8 eV energy, whereas the 470 nm fluorescence photon has 2.6 eV energy. The difference is converted to heat during the excimer formation and radiation processes. This results in 32% of the absorbed energy being converted to heat. Most absorption measurements were made with pump energies between 0.15 and 1.5 mJ, so the heat addition varied between 0.05 and 0.5 mJ. This was absorbed in a cylindrical volume having an average diameter of 1.5 mm and a length of 50 cm, so the excited volume was about 0.9 cm^3. Thus the heat loading, ΔE, varied between 0.06 and 0.6 J/ℓ. This must be compared to the heat energy of the gas, which is given by

$$E_H = \frac{3}{2} NkT \qquad (6.3.1)$$

At a temperature of 900 K and a gas density of 10^{19} cm^{-3}, E_H is calculated to be 190 J/ℓ. Therefore the fractional heat added is given by

$$3.2 \times 10^{-4} < \frac{\Delta E_H}{E_H} < 3.2 \times 10^{-3}. \qquad (6.3.2)$$

This is a small effect, which will lead to local temperature increases of the same magnitude. This will not be manifested as a density fluctuation until a time which is given by

$$t_c = \frac{d}{v_s} \qquad (6.3.3)$$

has elapsed. Here, d is the beam diameter and v_s is the sound velocity, which is given by

$$v_s = \sqrt{\frac{\gamma kT}{m}} , \qquad (6.3.4)$$

where γ is the ratio of specific heats, k is Boltzmann's constant, and m is the molecular mass. This is the time required for a shock wave traveling at the sound velocity to travel the diameter of the pump beam and establish a density gradient.

For an ideal, monatomic gas at 900 K, v_s is about 5×10^4 cm/sec. With d taken to be 1 mm, t_c is calculated to be 2 μs. However, the absorption is observed to appear almost simultaneously with the pump pulse, indicating it arises from a much faster process than the formation of a density gradient. Using reaction 2 in Table 4.1 and conditions typical for these experiments, excimers are formed at a rate

$$R = k_2 [Hg] [M]$$

or

$$R = 1 \times 10^7 \ s^{-1} \qquad (6.3.5)$$

The characteristic time is 1/R, or about 100 ns. This more closely matches the observed rise in absorption than does the estimated time to form a density gradient.

If the effect is due to an acoustic disturbance, it should be independent of wavelength. This is definitely not the case, as seen in Figure 6.7. Absorption is considerably less at 514.5 nm than at 457.9 nm.

There is the possibility that excited species create an anomalous dispersion which leads to defocusing of the probe beam. An estimate of defocusing caused by refractive index variation in the excited medium can be made following paraxial ray analysis given by Kogelnik and Li.[25] If the pump beam is assumed to induce an index variation which varies quadratically with the radial coordinate, r,

$$n(r) = n_0 - \frac{1}{2} n_2 r^2, \qquad (6.3.6)$$

then the appropriate ray transfer matrix for propagation through a length d of the excited medium is

$$\begin{pmatrix} A & B \\ C & D \end{pmatrix} = \begin{pmatrix} \cos(d\rho) & \frac{1}{\sqrt{n_0 n_2}} \sin(d\rho) \\ -\sqrt{n_0 n_2} \sin(d\rho) & \cos(d\rho) \end{pmatrix} \qquad (6.3.7)$$

where ρ is given by $\sqrt{n_2/n_0}$. In the present experiment, n_0 is very close to unity. This leads to defocusing by a "thermal lens" having a focal length

$$f = -\frac{1}{C} = \frac{1}{\sqrt{n_0 n_2} \sin(d\sqrt{n_2})} \qquad (6.3.8)$$

For small values of n_2, the focal length is approximately

$$f \approx \frac{1}{dn_2} \tag{6.3.9}$$

An appropriate expression for n_2 is found from[26]

$$n^2 \approx 1 + \frac{4\pi N|\mu|^2}{3hc\Delta\nu} \tag{6.3.10}$$

In Equation (6.3.10), $|\mu|$ is the electronic transition moment of a transition $\Delta\nu$ cm^{-1} away from the probe frequency. The excited state density, N, will have a radial dependence given by

$$N(r) = N_0 e^{-2(r/w_0)^2} \approx N_0 \left[1 - 2\left(\frac{r}{w_0}\right)^2\right], \tag{6.3.11}$$

where w_0 is the pump beam radius.

Substituting (6.3.11) into (6.3.10), and making the further assumption that the index variations are small gives

$$n(r) = 1 + \frac{2\pi N_0|\mu|^2}{3hc\Delta\nu} + \frac{4\pi N_0|\mu|^2}{3hc\Delta\nu w_0^2} r^2 \tag{6.3.12}$$

Comparing Equation (6.3.12) with Equation (6.3.6), it is seen that

$$n_0 = \frac{2\pi N_0|\mu|^2}{3hc\Delta\nu} \tag{6.3.13}$$

and

$$\frac{1}{2} n_2 = \frac{4\pi N_0|\mu|^2}{3hc\Delta\nu w_0^2} \tag{6.3.14}$$

For the case of a very strong transition, $|\mu|$ is on the order of 10^{-18} esu-cm. Assuming a detuning of 100 cm^{-1}, a beam radius of 0.05 cm, and an excited state density of 10^{15} cm^{-3}, then the index variation is found to be

$$n_2 \approx 1.7 \times 10^{-4} \text{ cm}^{-2} \tag{6.3.15}$$

Using this value in Equation (6.3.9) with d equal to 50 cm, the focal length of the "thermal lens" is found to be

$$f = 118 \text{ cm} \tag{6.3.16}$$

However, it is unlikely that the strengths of any nearby transitions are as as strong as 10^{-18} esu-cm, and the detuning factors will be larger than 100 cm^{-1} for most of the Ar^+ laser lines used to probe absorption. Therefore, the thermal lens will have a much longer focal length than that given by Equation (6.3.16).

Most absorption data was obtained with the probe beam focused loosely on a small area ($\approx$0.25 cm^2) solid state photodiode located about 5 m from the heated cell. One would expect that with such a long path length and with such small detectors, any significant density gradient defocusing would seriously deflect the beam and cause a large signal change. However, only small amplitude changes were observed. In any event, if defocusing was present, one would expect the effect to be reduced by placing a larger aperture detector closer to the cell. To check this, a 1P28 photomultiplier tube, having an area of about 1 cm x 1.5 cm was placed 50 cm from the cell. Although the signal was noisy, due to the discharge of the dye laser flashlamp circuitry, the absorption signal was definitely present and was approximately the same magnitude as that observed further away with smaller area detectors. Even if the thermal lensing effect is as great as that estimated in Equation (6.3.16), it would not be important in this last experiment.

In addition, if the signal decrease were due to a density disturbance in a shock wave propagating at the sound velocity, one might expect to observe effects from successive shock fronts as they reflect from the cell walls. These would occur at time intervals given by

$$t_r = \frac{d/2}{v_s} \qquad (6.3.17)$$

where d is the tube diameter. For d = 6 mm, t_r is found to be 6 μs. No such return shocks were ever observed.

It should be stated that under certain conditions it was possible to observe effects due to density gradients in our apparatus. These appeared as a slowly decaying intensity fluctuation when the pump and probe beams were not well aligned. The decay time for these signals was several milliseconds, and probably was determined by the thermal diffusion time of the disturbance. With the pump and probe beams carefully aligned, this effect was much smaller than the absorption signal. It is felt that any contributions to the signal caused by acoustic disturbances have been properly identified, and that the observed probe intensity decrease is due to absorption.

7.0 CONCLUSIONS

Since the absorption is present only when the pump laser is tuned to the cadmium resonance absorption, it seems likely that the cause is due to an excited state absorption in the CdHg excimer. Because absorption was only measured at specific argon ion laser wavelengths, it may be that there are regions in the fluorescence band which do not exhibit the effect. This could result if the absorption arises from a bound-bound transition rather than a bound-free transition. However, similar, continuous absorption is observed in the Hg_2^* 335 nm band.[27] If the same processes lead to absorption in $CdHg^*$ as in Hg_2^*, then the $CdHg^*$ absorption is probably continuous also.

Because of relativistic effects which are important in the heavier mercury atom, theorists have not yet calculated the electronic state structure of CdHg. However, it is possible to make some "educated guesses" about the CdHg electronic levels. For homonuclear systems, such as Hg_2, Cd_2, and Mg_2, there are four potential curves coming from the lowest $^3P + {}^1S$ atomic asymptote. In the case of Mg_2, these are the $^3\Pi_g$ (bound), $^3\Sigma_u$ (bound), $^3\Pi_u$ (unbound), and $^3\Sigma_g$ (unbound) states.[28] For Hg_2, spin-orbit coupling becomes more important, and these states are now designated by the principle quantum number, Ω, according to the following notation.[29]

$^3\Sigma_g$	becomes	$1_g, 0_g^-$
$^3\Pi_u$	becomes	$2_u, 1_u, 0_u^+$
$^3\Sigma_u$	becomes	$1_u, 0_u^-$
$^3\Pi_u$	becomes	$2_g, 1_g, 0_g^+$

In a heteronuclear molecule, such as CdHg, this asymptote splits into asymptotes corresponding to the Cd ($^3P_{0,1,2}$) + Hg ($^1S_0$) and Cd ($^1S_0$) + Hg ($^3P_{0,1}$) atomic states. Also, due to lack of nuclear symmetry, the u, g state designation does not exist. The first of these gives rise to the bound CdHg excimer states, while the second which lies at a higher energy, could give rise to several unbound states. These unbound states may lie at an approximate energy to cause absorption at 470 nm.[29] The next higher atomic asymptotes are the Hg ($^1S_0$) + Cd ($^1P_1$) and Hg ($^3P_2$) + Cd ($^1S_0$) states. The first of these should form bound

states which could lead to absorption in the 470 nm wavelength region.[29] The second asymptote should form unbound states which lie at too high energy to cause absorption. Figure 7.1 shows some of the possible excited states of CdHg which could absorb in the wavelength region where laser action was anticipated.

Absorption cross sections for a transition to states arising from the Hg($^1S_0$) + Cd ($^1P_1$) asymptote should be small. This is because the absorption should occur to vibrational levels near the dissociation asymptote and thus, the Franck-Condon factors will be small. Absorption to the 0^+ state arising from the Hg ($^3P_1$) + Cd ($^1S_0$) asymptote would probably have a larger cross section, and would also have a continuous wavelength dependence. A third electronic state which could possibly absorb near 470 nm is indicated by the dashed curve in Figure 7.1. If a bound state having approximately 1 eV binding energy originates from the Hg ($^1S_0$) + Cd ($^3S_1$) asymptote, then this is also a possibly absorbing transition. The above discussion is somewhat speculative, but it is included to show that absorptions near 470 nm are possible in the excited electronic states of CdHg. A more definitive examination of the subject must depend on better calculations of the CdHg electronic levels and their associated transition moments.

The measurements performed under this program cast considerable doubt on the possibility of efficient laser action in CdHg. If further studies are conducted, they should investigate the cause of the absorption, with the hope of finding a way to avoid it.

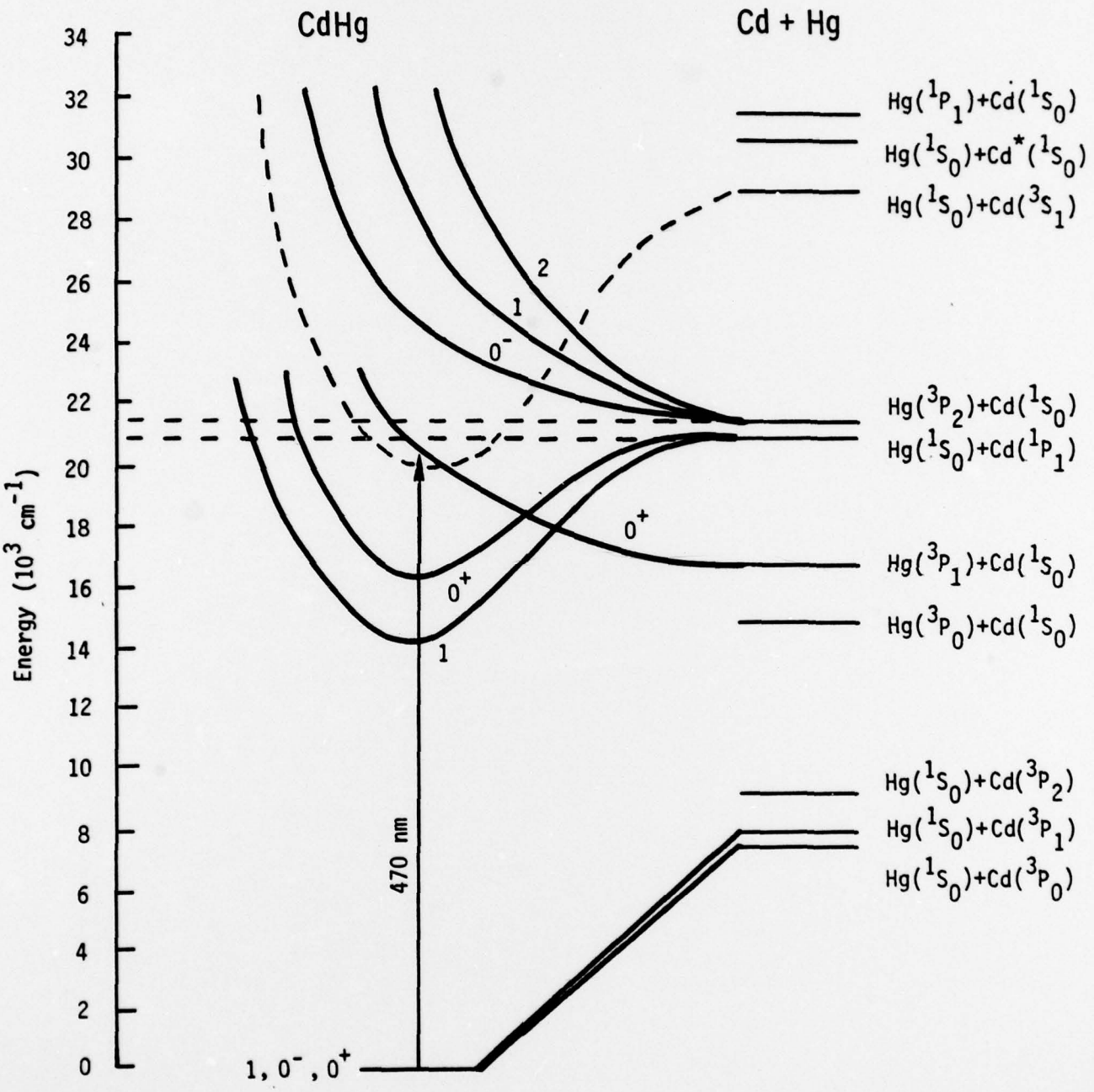

Figure 7.1 Excited CdHg Electronic States

8.0 REFERENCES

1. R. S. Bradford, Jr., W. B. Lacina, E. R. Ault, and M. L. Bhaumik, "High Efficiency Discharge Excitation of the KrF Laser," Opt. Commun. 18, 210 (1976).

2. M. L. Bhaumik, R. S. Bradford, Jr., and E. R. Ault, "High Efficiency KrF Excimer Laser," Appl. Phys. Lett. 28, 23 (1976).

3. M. W. McGeoch, G. R. Fournier, and P. Ewart, "Visible Continua of the Cadmium Mercury Molecule," J. Phys. B 9, L121 (1976).

4. G. R. Fournier and M. W. McGeoch, "Kinetics of the Proposed Cadmium Mercury Excimer," Opt. Commun. 18, 121 (1976).

5. G. R. Fournier and M. W. McGeoch, "Kinetic Model of the Sustained Discharge Excitation of the Cadmium Mercury Excimer," J. Appl. Phys. 49, 2651 (1978).

6. M. W. McGeoch and G. R. Fournier, "Positive Gain Measurements on the 470 nm Continuum Band of CdHg," J. Appl. Phys. 49, 2659 (1978).

7. D. Drummond and L. A. Schlie, "The Thallium Mercury Excimer and its Potential as a Laser," J. Chem. Phys. 65. 3454 (1976).

8. L. Pleasance, private communication.

9. W. H. Breckenridge, T. W. Broadbent, and D. S. Moore, "A Determination by Resonance Radiation Flash Photolysis of the Absolute Reaction Rates of Excited Cadmium Atoms with Several Gases," J. Phys. Chem. 79. June 19, 1975.

10. T. Holstein, "Imprisonment of Resonance Radiation in Gases," Phys. Rev. 72, Dec. 15, 1947, and Phys. Rev. 83, Sept. 15, 1951.

11. R. H. Springer and B. T. Barnes, "Intensities of 2288A and 3261A Radiation from Low Pressure Cadmium Rare Gas Discharges," J. Appl. Phys. 39, (1968).

12. R. B. Miles, "Optical Third Harmonic Generation in Metal Vapors," M. L. Report No. 2069, Stanford University, June 1972.

13. T. M. Bieniewski, "Collision Broadening of Spectral Lines by Identical Atoms," Atomic Collision Processes, Amsterdam, North Holland Publishing Co., 1964, p. 1055.

14. S. J. Holmes, private communication.

15. E. A. Stappaerts, "Infrared Image Up-Conversion in Alkali Metal Vapors," G. L. Report No. 2569, Stanford University, May 1976.

16. A. Javan and P. L. Kelley, "Possibility of Self-Focusing due to Intensity Dependent Anomalous Dispersion," IEEE J. Quant. Electron. QE-2 (1966).

17. J. N. Elgin, G. H. C. New, and K. E. Orkney, "Generalized Semiclassical Fromalism for Two-Photon Resonant Problems," Opt. Commun. (in press).

18. C. H. Corliss and W. R. Bozman, "Experimental Transition Probabilities for Spectral Lines of Seventy Elements," NBS Monograph 53.

19. G. V. Marr, "Photoionization Processes in Gases," Academic Press, New York, 1967.

20. R. E. Honig and D. A. Kramer, "Vapor Pressure Data for the Solid and Liquid Elements," RCA Rev., p. 285, June 1969.

21. A. N. Nesmeyanov, Vapor Pressure of the Chemical Elements, Elsevier Publishing Co., New York, 1963, p. 201.

22. T. F. Ewanizky, "An Unstable Resonator Flashlamp Pumped Dye Laser," App. Phys. Lett. 25, 295 (1974).

23. U. Ganiel, A. Hardy, and D. Traves, "Analysis of Injection Locking in Pulsed Dye Laser Systems," IEEE J. Quant. Electron QE-12, 704 (1976).

24. R. E. Drullinger and M. Stock, "The Cd_2^* Excimer: Fluorescence Band Shape and Decay Rates," J. Chem. Phys. 68, 5299 (1978).

25. H. Kogelnik and T. Li, "Laser Beams and Resonators," Proc. IEEE 54, 1312 (1966).

26. S. S. Penner, Quantitative Molecular Spectroscopy and Gas Emissivities, Addison-Wesley Publishing Co., Inc., Reading, Mass. (1959), p. 228.

27. R. E. Center and S. E. Moody, "Optical Studies in High Pressure Mercury Discharges," paper presented at Thirty First Gaseous Electronics Conference, Buffalo, New York, October 1978.

28. W. J. Stevens and M. Krauss,"The Electronic Structure of the Ground and Excited States of Mg_2^+ and Mg_2," J. Chem. Phys. 67, 1977 (1977).

29. W. J. Stevens and M. Krauss, private communication.